

March 2021

Simulations of the Angular Recoil–Energy Distribution of WIMP–Scattered Target Nuclei for Directional Dark Matter Detection Experiments

CHUNG-LIN SHAN

*Preparatory Office of the Supporting Center for Taiwan Independent Researchers
P.O.BOX 21 National Yang Ming Chiao Tung University, Hsinchu City 30099, Taiwan, R.O.C.*

E-mail: clshan@tir.tw

Abstract

In this paper, as the second part of the third step of our study on developing data analysis procedures for using 3-dimensional information offered by directional direct Dark Matter detection experiments in the future, we investigate the angular distributions of the recoil direction (flux) and the recoil energy of the Monte Carlo simulated WIMP–scattered target nuclei observed in different celestial coordinate systems. The “anisotropy” and the “directionality” (“annual” modulation) of the angular recoil–direction/energy distributions will be demonstrated. We will also discuss their dependences on the target nucleus and on the mass of incident halo WIMPs. For readers’ reference, all simulation plots presented in this paper (and more) can be found “in animation” on our online (interactive) demonstration webpage (<http://www.tir.tw/phys/hep/dm/amidas-2d/>).

arXiv:2103.06486v1 [hep-ph] 11 Mar 2021

1 Introduction

In the last (more than) three decades, a large number of experiments has been built and is being planned to search for the most favorite Dark Matter (DM) candidate: Weakly Interacting Massive Particles (WIMPs) χ , by direct detection of the scattering recoil energy of ambient WIMPs off target nuclei in low-background underground laboratory detectors (see Refs. [1, 2, 3, 4] for reviews).

Besides non-directional direct detection experiments measuring only recoil energies deposited in detectors, the “directional” detection of Galactic DM particles has been proposed more than one decade to be a promising experimental strategy for discriminating signals from backgrounds by using additional 3-dimensional information (recoil tracks and/or head-tail senses) of (elastic) WIMP-nucleus scattering events (see Refs. [5, 6, 7, 8, 9] for reviews and recent progresses).

As the preparation for our future study on the development of data analysis procedures for using and/or combining 3-D information offered by directional Dark Matter detection experiments to, e.g., reconstruct the 3-dimensional WIMP velocity distribution, in Ref. [10], we started with the Monte Carlo generation of the 3-D velocity of (incident) halo WIMPs in the Galactic coordinate system, including the magnitude, the direction, and the incoming/scattering time. Each generated 3-D WIMP velocity has then been transformed to the laboratory-independent (Ecliptic, Equatorial, and Earth) coordinate systems as well as to the laboratory-dependent (horizontal and laboratory) coordinate systems (see the simulation workflow sketched in Fig. 1) for the investigations on the angular distribution patterns of the 3-D WIMP velocity (flux) and the (accumulated and average) kinetic energy in different celestial coordinate systems [10, 11] as well as the Bayesian reconstruction of the radial component (magnitude) of the 3-D WIMP velocity [10]. Not only the diurnal modulations, we demonstrated also the “annual” modulations of the angular WIMP velocity (flux)/kinetic-energy distributions [10, 11].

However, besides recoil energies, what one could measure (directly) in directional DM detection experiments is recoil tracks (with the sense-recognition) and in turn recoil angles (directions) of scattered target nuclei. In Ref. [12], we have finally achieved our double-Monte Carlo scattering-by-scattering simulation of the 3-D elastic WIMP-nucleus scattering process and can provide the 3-D recoil direction and then the recoil energy of the WIMP-scattered target nuclei event by event in different celestial coordinate systems. In this paper, we focus at first on the simulation results of the angular distributions of the recoil direction (flux) as well as the accumulated and the average recoil energies of the target nuclei scattered by incident halo WIMPs (circled in the simulation workflow in Fig. 1). An investigation on the 3-D *effective* velocity and kinetic energy distributions of halo WIMPs *scattering off* target nuclei in an underground detector (indicated by the upper solid blue arrow in Fig. 1) will be presented in Ref. [13] separately.

The remainder of this paper is organized as follows. In Sec. 2, we describe the overall workflow of our double-Monte Carlo scattering-by-scattering simulation procedure of 3-dimensional elastic WIMP-nucleus scattering as well as introduce an incoming-WIMP coordinate system and discuss the validation criterion of our MC simulation of 3-D WIMP scattering events. Then, in Secs. 3, 4, and 5, we demonstrate the angular distributions of the recoil direction (flux) as well as the accumulated and the average recoil energies of scattered target nuclei observed in the incoming-WIMP, the laboratory-dependent laboratory, and the laboratory-independent Equatorial coordinate systems, respectively. Their target and WIMP-mass dependences as well as the annual modulations will also be discussed in detail. We conclude in Sec. 6.

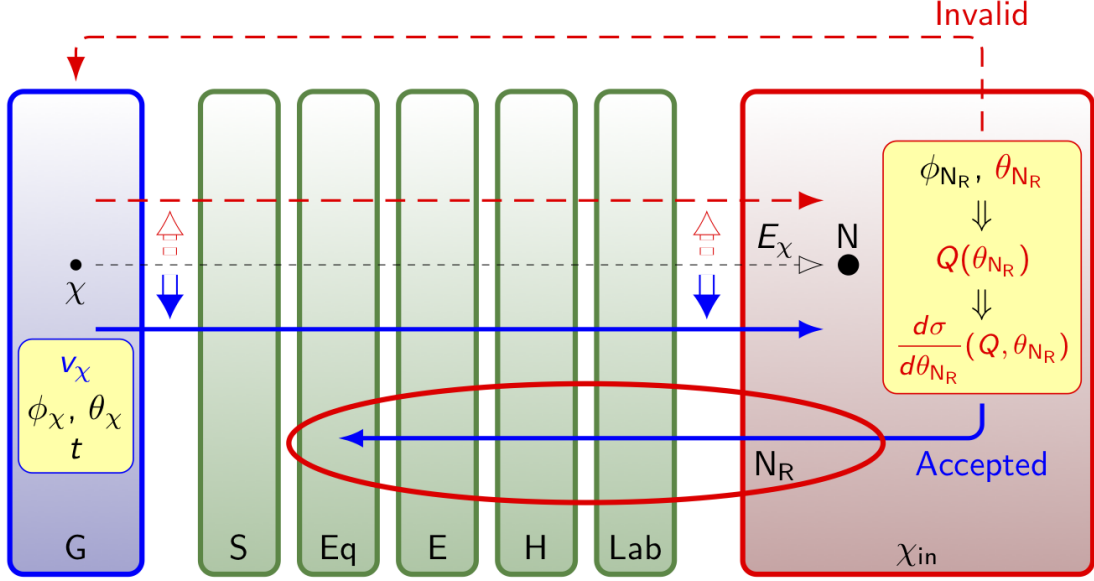


Figure 1: The workflow of our double–Monte Carlo simulation and data analysis procedure of 3-dimensional elastic WIMP–nucleus scattering. See the text for detailed descriptions.

2 Monte Carlo scattering–by–scattering simulation of 3-dimensional elastic WIMP–nucleus scattering events

In Ref. [12], we have

1. reviewed the MC generation of the 3-D velocity information (the magnitude, the direction, and the incoming/scattering time) of Galactic WIMPs,
2. summarized the definitions of and the transformations between all celestial coordinate systems.

In this section, we focus then on the core part of our simulation procedure: the generation and the validation of 3-D elastic WIMP–nucleus scattering events in the “incoming–WIMP” coordinate system.

We describe at first the overall workflow of our Monte Carlo scattering–by–scattering simulation of the 3-D elastic WIMP–nucleus scattering process. Then we give our definition of the incoming–WIMP coordinate system as well as those of (the orientation of) the scattering plane and the (equivalent) recoil angle. At the end we discuss the validation criterion of our Monte Carlo simulations by taking into account the cross section (nuclear form factor) suppression on *each* generated recoil energy.

2.1 Simulation workflow

In this subsection, we describe the overall workflow of our double–Monte Carlo simulation and data analysis procedure of 3-D elastic WIMP–nucleus scattering sketched in Fig. 1 in detail:

1. The 3-D velocity information of incident halo WIMPs (the magnitude and the direction as well as the incoming/scattering time) is MC generated according to a specified model of the Dark Matter halo in the Galactic coordinate system (the blue subframe) [10, 12].

2. The generated 3-D WIMP velocities will be transformed through the laboratory-independent (Ecliptic, Equatorial, and Earth) coordinate systems as well as the laboratory-dependent (horizontal and laboratory) coordinate systems (the green subframes) [10, 12] and at the end into the incoming-WIMP coordinate system (the red subframe, defined in Sec. 2.2).
3. In the incoming-WIMP coordinate system, the 3-D elastic WIMP-nucleus scattering process will also be MC simulated by generating the orientation of the scattering plane $\phi_{N_R, \chi_{in}}$ and the “equivalent” recoil angle $\theta_{N_R, \chi_{in}}$ (defined in Sec. 2.3). They define the recoil direction of the scattered target nucleus and the latter, combined with the transformed WIMP incident velocity, will then be used for estimating the transferred recoil energy to the target nucleus, $Q(\theta_{N_R, \chi_{in}})$, and the differential WIMP-nucleus scattering cross section with respect to the recoil angle, $d\sigma/d\theta_{N_R, \chi_{in}}(Q, \theta_{N_R, \chi_{in}})$, in our event validation criterion (see Sec. 2.3 for details).
4. The orientation of the scattering plane $\phi_{N_R, \chi_{in}}$ and the equivalent recoil angle $\theta_{N_R, \chi_{in}}$ of the *accepted* recoil events will be transformed (back) through all considered celestial coordinate systems (indicated by the lower solid blue arrow). All these 3-D recoil information of the scattered target nucleus accompanied with the corresponding recoil energy Q as well as the 3-D velocity of the scattering WIMP in different coordinate systems (the upper solid blue arrow) will be recorded for further analyses¹.
5. For the *invalid* cases, in which the estimated recoil energies are out of the experimental measurable energy window or suppressed by the validation criterion, the generated 3-D information on the incident WIMP (the lower dashed red arrow) (and that on the scattered nucleus) will be discarded and the generation/validation process of one WIMP scattering event will be restarted from the Galactic coordinate system (the upper dashed red arrow).

2.2 Definition of the incoming-WIMP coordinate system

In Fig. 2, we sketch the definition of the (light-green) incoming-WIMP coordinate system in the (dark-green) laboratory coordinate system. Note that, practically, the center of the incoming-WIMP coordinate system is at the position of the scattered target nucleus before scattering (see Fig. 3). The $\mathbf{Z}_{\chi_{in}}$ -axis is defined as usual as the direction of the incident velocity of the incoming WIMP \mathbf{v}_χ . $\phi_{\chi, \text{Lab}}$ and $\theta_{\chi, \text{Lab}}$ indicate the azimuthal angle and the elevation of the direction of \mathbf{v}_χ measured in the laboratory coordinate system, respectively. The $\mathbf{X}_{\chi_{in}}$ -axis is perpendicular to the $\mathbf{Z}_{\chi_{in}}$ -axis and lies on the $\mathbf{Z}_{\text{Lab}}-\mathbf{Z}_{\chi_{in}}$ plane. Then the $\mathbf{Y}_{\chi_{in}}$ -axis is defined by the right-handed convention.

Note that, in our Monte Carlo simulations of 3-D elastic WIMP-nucleus scattering, the velocity (incident direction) of halo WIMPs in the laboratory and the Equatorial coordinate systems as well as the $\mathbf{Z}_{\chi_{in}}$ -axis of the incoming-WIMP coordinate system are *not fixed* as from the direction of the CYGNUS constellation. Interested readers can refer to Ref. [10] for the detailed discussions about (the annual and the diurnal modulations of) the anisotropy of the angular distributions of the 3-D WIMP velocity (flux) in the laboratory and the Equatorial coordinate systems.

¹In this paper, we focus on investigating the angular distributions of the nuclear recoil direction (flux)/energy (indicated by the lower blue arrow). A detailed study on the 3-dimensional effective velocity distribution of the incident WIMPs scattering off target nuclei (the upper blue arrow) is presented in Ref. [13] separately.

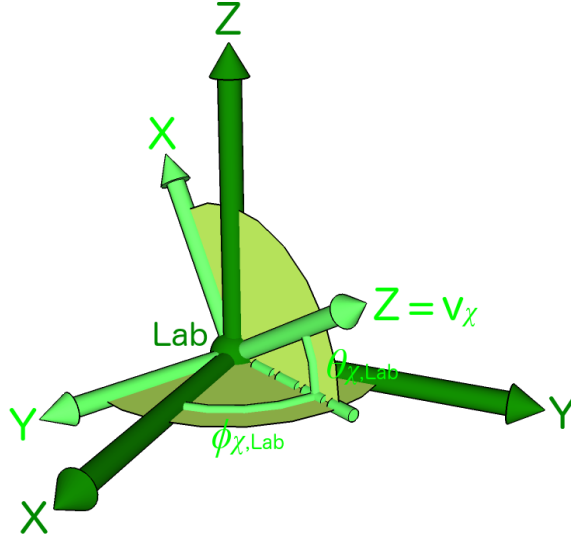


Figure 2: The definition of the (light–green) incoming–WIMP coordinate system in the (dark–green) laboratory coordinate system. The $\mathbf{Z}_{\chi_{\text{in}}}$ –axis is defined as usual as the direction of the incident velocity of the incoming WIMP \mathbf{v}_{χ} . $\phi_{\chi,\text{Lab}}$ and $\theta_{\chi,\text{Lab}}$ indicate the azimuthal angle and the elevation of the direction of \mathbf{v}_{χ} measured in the laboratory coordinate system, respectively. The $\mathbf{X}_{\chi_{\text{in}}}$ –axis is perpendicular to the $\mathbf{Z}_{\chi_{\text{in}}}$ –axis and lies on the $\mathbf{Z}_{\text{Lab}}\text{--}\mathbf{Z}_{\chi_{\text{in}}}$ plane. Then the $\mathbf{Y}_{\chi_{\text{in}}}$ –axis is defined by the right–handed convention.

2.3 Generation of nuclear recoil directions

In Fig. 3, we sketch the process of one single 3-D elastic WIMP–nucleus scattering event: $\chi_{\text{in/out}}$ indicate the incoming and the outgoing WIMPs, respectively. While ζ indicates the scattering angle of the outgoing WIMP χ_{out} (measured from the $\mathbf{Z}_{\chi_{\text{in}}}$ –axis), η is the recoil angle of the scattered target nucleus N_{R} .

It can be found firstly that the orientation of the $(\mathbf{v}_{\chi_{\text{out}}}\text{--}\mathbf{Z}_{\chi_{\text{in}}}\text{--}\mathbf{v}_{\text{N}_{\text{R}}})$ scattering plane of *this single* scattering event can be specified by the azimuthal angle of the recoil direction of the scattered nucleus, $\phi_{\text{N}_{\text{R}},\chi_{\text{in}}}$, which should be azimuthal symmetric around the $\mathbf{Z}_{\chi_{\text{in}}}$ –axis and is thus generated with a constant probability in our simulations:

$$f_{\text{N}_{\text{R}},\chi_{\text{in}},\phi}(\phi_{\text{N}_{\text{R}},\chi_{\text{in}}}) = 1, \quad \phi_{\text{N}_{\text{R}},\chi_{\text{in}}} \in (-\pi, \pi]. \quad (1)$$

On the other hand, the elevation of the recoil direction of the scattered nucleus, $\theta_{\text{N}_{\text{R}},\chi_{\text{in}}}$, is namely the complementary angle of the recoil angle η and we thus use

$$\theta_{\text{N}_{\text{R}},\chi_{\text{in}}} \in [0, \pi/2] \quad (2)$$

as the “equivalent” recoil angle in our simulations². Since for one WIMP event transformed into the laboratory coordinate system with the velocity of $\mathbf{v}_{\chi}(v_{\chi,\text{Lab}}, \phi_{\chi,\text{Lab}}, \theta_{\chi,\text{Lab}})$, the kinetic energy can be given by

$$E_{\chi} = \frac{1}{2}m_{\chi}|\mathbf{v}_{\chi}|^2 = \frac{1}{2}m_{\chi}v_{\chi,\text{Lab}}^2. \quad (3)$$

²Note that, without special remark, we will use hereafter simply “the recoil angle” to indicate “the equivalent recoil angle $\theta_{\text{N}_{\text{R}},\chi_{\text{in}}}$ ” (not η).

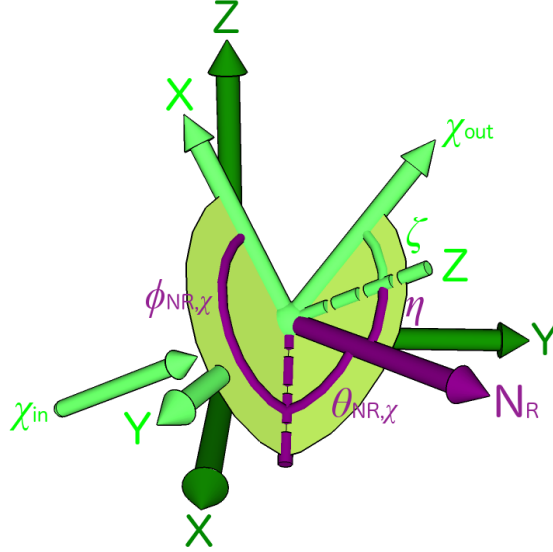


Figure 3: A 3-D elastic WIMP–nucleus scattering event in the (light–green) incoming–WIMP and the (dark–green) laboratory coordinate systems. ζ and η are the scattering angle of the outgoing WIMP χ_{out} and the recoil angle of the scattered target nucleus N_{R} measured in the incoming–WIMP coordinate system of *this single* scattering event, respectively. While the azimuthal angle of the recoil direction of the scattered nucleus N_{R} in this incoming–WIMP coordinate system, $\phi_{N_{\text{R}},\chi_{\text{in}}}$, indicates the orientation of the scattering plane, the elevation of the recoil direction of N_{R} , $\theta_{N_{\text{R}},\chi_{\text{in}}}$, is namely the complementary angle of the recoil angle η .

Then the recoil energy of the scattered target nucleus in the incoming–WIMP coordinate system can be estimated by the equivalent recoil angle $\theta_{N_{\text{R}},\chi_{\text{in}}}$ as [12]

$$Q(\theta_{N_{\text{R}},\chi_{\text{in}}}) = \left[\left(\frac{2m_{\text{r},\text{N}}^2}{m_{\text{N}}} \right) v_{\chi,\text{Lab}}^2 \right] \sin^2(\theta_{N_{\text{R}},\chi_{\text{in}}}), \quad (4)$$

where $m_{\text{r},\text{N}} \equiv m_{\chi}m_{\text{N}}/(m_{\chi} + m_{\text{N}})$ is the reduced mass of the WIMP mass m_{χ} and that of the target nucleus m_{N} . And the differential cross section $d\sigma$ given by the absolute value of the momentum transfer from the incident WIMP to the recoiling target nucleus, $q = |\mathbf{q}| = \sqrt{2m_{\text{N}}Q}$, can be obtained as [1, 12]

$$d\sigma = \frac{1}{v_{\chi,\text{Lab}}^2} \left(\frac{\sigma_0}{4m_{\text{r},\text{N}}^2} \right) F^2(q) dq^2 = \sigma_0 F^2(Q(\theta_{N_{\text{R}},\chi_{\text{in}}})) \sin(2\theta_{N_{\text{R}},\chi_{\text{in}}}) d\theta_{N_{\text{R}},\chi_{\text{in}}}. \quad (5)$$

Hence, the differential WIMP–nucleus scattering cross section with respect to the recoil angle $\theta_{N_{\text{R}},\chi_{\text{in}}}$ can generally be given by [12]³

$$\frac{d\sigma}{d\theta_{N_{\text{R}},\chi_{\text{in}}}} = \left[\sigma_0^{\text{SI}} F_{\text{SI}}^2(Q(\theta_{N_{\text{R}},\chi_{\text{in}}})) + \sigma_0^{\text{SD}} F_{\text{SD}}^2(Q(\theta_{N_{\text{R}},\chi_{\text{in}}})) \right] \sin(2\theta_{N_{\text{R}},\chi_{\text{in}}}). \quad (6)$$

Here $\sigma_0^{(\text{SI},\text{SD})}$ are the spin–independent (SI)/spin–dependent (SD) total cross sections ignoring the form factor suppression and $F_{(\text{SI},\text{SD})}(Q)$ indicate the elastic nuclear form factors corresponding to the SI/SD WIMP interactions, respectively.

³It would be important to emphasize here that, to the best of our knowledge, this should be the first time in literature that some constraints on the nuclear recoil angle/direction caused by (elastic) WIMP–nucleus scattering cross sections (nuclear form factors) have been considered in (3-D) WIMP scattering simulations.

Finally, taking into account the proportionality of the WIMP flux to the incident velocity, the generating probability distribution of the recoil angle $\theta_{\text{NR},\chi_{\text{in}}}$, which is proportional to the scattering event rate of incident halo WIMPs with an incoming velocity $v_{\chi,\text{Lab}}$ off target nuclei going into recoil angles of $\theta_{\text{NR},\chi_{\text{in}}} \pm d\theta_{\text{NR},\chi_{\text{in}}}/2$ with recoil energies of $Q \pm dQ/2$, can generally be given by [12]

$$f_{\text{NR},\chi_{\text{in}},\theta}(\theta_{\text{NR},\chi_{\text{in}}}) = \left(\frac{v_{\chi,\text{Lab}}}{v_{\chi,\text{cutoff}}} \right) \left[\sigma_0^{\text{SI}} F_{\text{SI}}^2(Q(\theta_{\text{NR},\chi_{\text{in}}})) + \sigma_0^{\text{SD}} F_{\text{SD}}^2(Q(\theta_{\text{NR},\chi_{\text{in}}})) \right] \sin(2\theta_{\text{NR},\chi_{\text{in}}}), \quad (7)$$

where $v_{\chi,\text{cutoff}} \simeq 800$ km/s is a cut-off velocity of incident halo WIMPs in the laboratory coordinate system.

3 Angular distributions of the recoil direction/energy in the incoming-WIMP frame

In Refs. [10] and [11], we demonstrated the angular distributions of the 3-D velocity (flux) and the kinetic energy of Galactic halo WIMPs impinging into (directional) direct DM detectors in different celestial coordinate systems, which show clearly the anisotropy and the directionality (the annual and/or the diurnal modulations). Since what we can practically observe (reconstruct) in directional Dark Matter detection experiments is the recoil energies and the recoil tracks (and the head-tail senses) of target nuclei, in this and the next two sections, we discuss the angular distributions of the recoil direction (flux) as well as the accumulated and the average recoil energies of target nuclei scattered by (simulated) incident Galactic WIMPs observed in the incoming-WIMP, the laboratory-dependent laboratory, and the laboratory-independent Equatorial coordinate systems, respectively.

Three spin-sensitive nuclei used frequently in (directional) direct detection experiments: ^{19}F , ^{73}Ge , and ^{129}Xe have been considered as our targets⁴. Then, while the SI (scalar) WIMP-nucleon cross section has been fixed as $\sigma_{\chi\text{p}}^{\text{SI}} = 10^{-9}$ pb in our simulations presented in this paper, the effective SD (axial-vector) WIMP-proton/neutron couplings have been tuned as $a_{\text{p}} = 0.01$ and $a_{\text{n}} = 0.7a_{\text{p}} = 0.007$, respectively [12]. So that the contributions of the SI and the SD WIMP-nucleus cross sections (including the corresponding nuclear form factors) to the validation criterion (7) are approximately comparable for the considered ^{73}Ge and ^{129}Xe target nuclei⁵.

Moreover, in this paper we assume simply that the experimental threshold energies for all considered target nuclei are negligible, whereas the maximal experimental cut-off energy has been set as $Q_{\text{max}} = 100$ keV. 5,000 experiments with 500 accepted events on average (Poisson-distributed) in one observation period (365 days/year or 60 days/season) in one experiment for one laboratory/target nucleus have been simulated.

For readers' reference, all simulation plots presented in this paper (and more) can be found "in animation" on our online (interactive) demonstration webpage [14].

⁴Although Ge and Xe are (so far) not used in directional detection experiments, for readers' cross reference to Ref. [13], we present simulations with them here, which would show similar results as with the $^{79/81}\text{Br}$ and ^{127}I nuclei, respectively.

⁵The mass of the ^{19}F nucleus is too light. Thus, with the same simulation setup, the SD WIMP-nucleus cross section dominates.

3.1 Angular distributions of the recoil direction/energy of light target nuclei

In this subsection, we present at first the angular distributions of the recoil direction (flux) as well as the accumulated and the average recoil energies of light target nuclei in the incoming–WIMP coordinate system.

In the left column of Figs. 4, we show the angular distributions of the recoil direction (flux) (top), the accumulated (middle) and the average (bottom) recoil energies of ^{19}F in unit of the all–sky average values. (Note that the scale of the color bar used in the bottom frame is different from that in the top and the middle frames.) Meanwhile, the corresponding event number (top), the accumulated (middle) and the average (bottom) recoil energies of ^{19}F as functions of the recoil angle $\theta_{\text{NR},\chi_{\text{in}}}$ have also been provided in the right column, where the thin vertical dashed black lines indicate the 1σ statistical uncertainties. The mass of incident WIMPs has been set as $m_\chi = 100$ GeV. 500 accepted WIMP scattering events on average in one entire year have been simulated and binned into 12×12 bins for the azimuthal angle and the elevation (left) and 12 bins in the range of $\theta_{\text{NR},\chi_{\text{in}}} = 0$ and 90° (right), respectively.

As a reference, in the plots shown in the right column, we draw also the dash–dotted red and the dash–double–dotted blue curves to indicate two theoretical cases: all WIMPs move monotonically with the root–mean–square velocity [12]

$$v_{\text{rms,Lab}}^2 = \left(\frac{3}{2}\right) v_0^2 + v_e^2 \simeq (355 \text{ km/s})^2, \quad (8)$$

namely, carry the average kinetic energy

$$\langle E_\chi \rangle = \left(\frac{1}{2}\right) m_\chi v_{\text{rms,Lab}}^2, \quad (9)$$

and all WIMPs carry only $\langle E_\chi \rangle / 2$ (with the common velocity of $v_{\text{rms,Lab}}/\sqrt{2} \simeq 250$ km/s), respectively. Additionally, the quadruple–dotted green curve in the top–right frame is the exact $\sin(2\theta_{\text{NR},\chi_{\text{in}}})$ curve, which indicates the case of *zero* cross section (nuclear form factor) suppression considered in the validation criterion (7).

First of all, it can be seen that, since the $\mathbf{Z}_{\chi_{\text{in}}}$ –axis (of each accepted WIMP–nucleus scattering event) is defined as the incident direction of the incoming WIMP, the angular distributions of the recoil direction as well as the accumulated/average recoil energies (of the ^{19}F target) in the left column of Figs. 4 show not surprisingly the “azimuthal symmetry”. However, as one can also find in the right column, the most frequent and the most energetic recoil directions (angles) do *not* appear around the $+\mathbf{Z}_{\chi_{\text{in}}}$ –axis ($\theta_{\text{NR},\chi_{\text{in}}} = 90^\circ$), but around the angle of $\theta_{\text{NR},\chi_{\text{in}}} \simeq 45^\circ$ and $\theta_{\text{NR},\chi_{\text{in}}} \simeq 60^\circ$, respectively! More precisely, due to the factor of $\sin(2\theta_{\text{NR},\chi_{\text{in}}})$ in the expression (7) for $f_{\text{NR},\chi_{\text{in}},\theta}(\theta_{\text{NR},\chi_{\text{in}}})$ and the proportionality of the recoil energy Q to $\sin^2(\theta_{\text{NR},\chi_{\text{in}}})$, $\theta_{\text{NR},\chi_{\text{in},\text{max}}} = 45^\circ$ and $\theta_{\text{NR},\chi_{\text{in},\text{Qmax}}} = 60^\circ$ are the *upper* bounds of the most frequent and the most energetic recoil angles, respectively. And, as we will demonstrate later, the most frequent/energetic recoil angles move towards (much) smaller $\theta_{\text{NR},\chi_{\text{in}}}$, when the mass of the target nucleus and/or incident WIMPs becomes heavier.

Moreover, the recoil–angle distribution $f_{\text{NR},\chi_{\text{in}},\theta}(\theta_{\text{NR},\chi_{\text{in}}})$ of ^{19}F nuclei scattered by 100–GeV WIMPs shown in the top–right frame of Figs. 4 matches almost (but not) perfectly the dash–dotted red average–kinetic–energy curve (as well as the dash–double–dotted blue half–average–kinetic–energy and the quadruple–dotted green zero–form–factor–suppression curves⁶). This

⁶As shown in Fig. 5 and will be discussed in detail later, this is due to the (relatively) pretty flat decrease of the scattering cross section (nuclear form factor) of the ^{19}F target with the increased recoil energy.

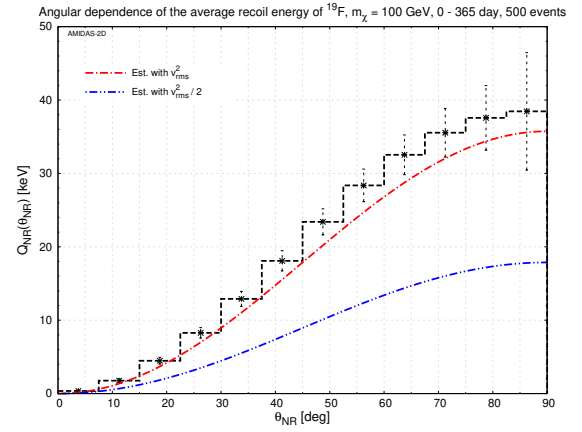
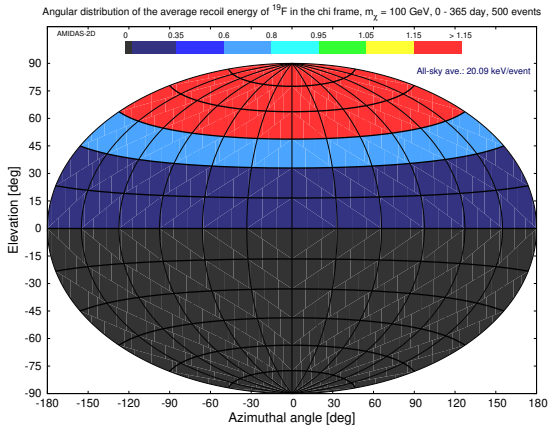
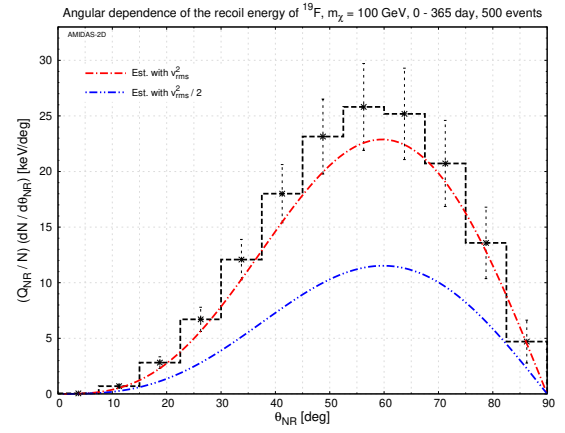
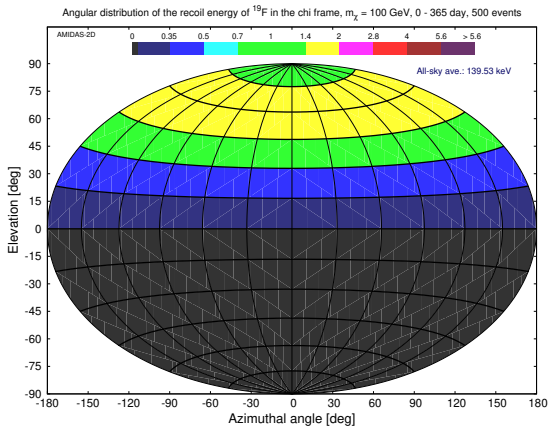
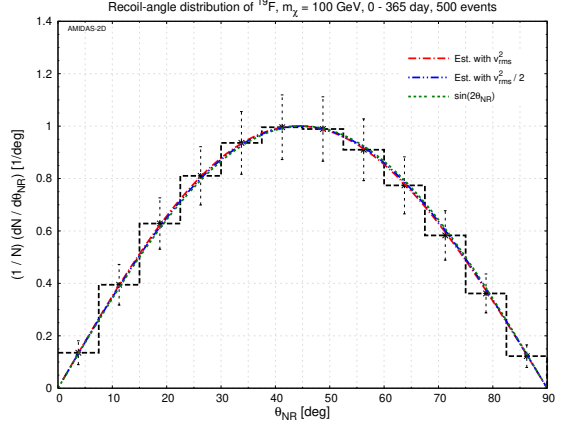
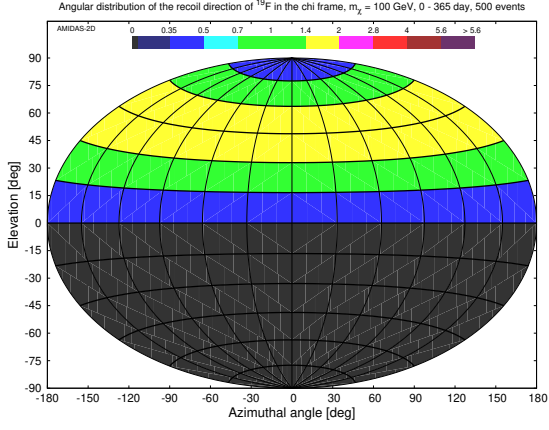


Figure 4: Left: the angular distributions of the recoil direction (flux) (top), the accumulated (middle) and the average (bottom) recoil energies of ^{19}F in unit of the all-sky average values. (Note that the scale of the color bar used in the bottom frame is different from that in the top and the middle frames.) Right: the recoil-angle $\theta_{\text{NR},\chi_{\text{in}}}$ dependences of the corresponding event number (top), the accumulated (middle) and the average (bottom) recoil energies of ^{19}F ; the thin vertical dashed black lines indicate the 1σ statistical uncertainties. The mass of incident WIMPs has been set as $m_\chi = 100$ GeV. 500 accepted WIMP scattering events on average in one entire year have been simulated and binned into 12×12 bins for the azimuthal angle and the elevation (left) and 12 bins in the range of $\theta_{\text{NR},\chi_{\text{in}}} = 0$ and 90° (right), respectively. See the text for further details.

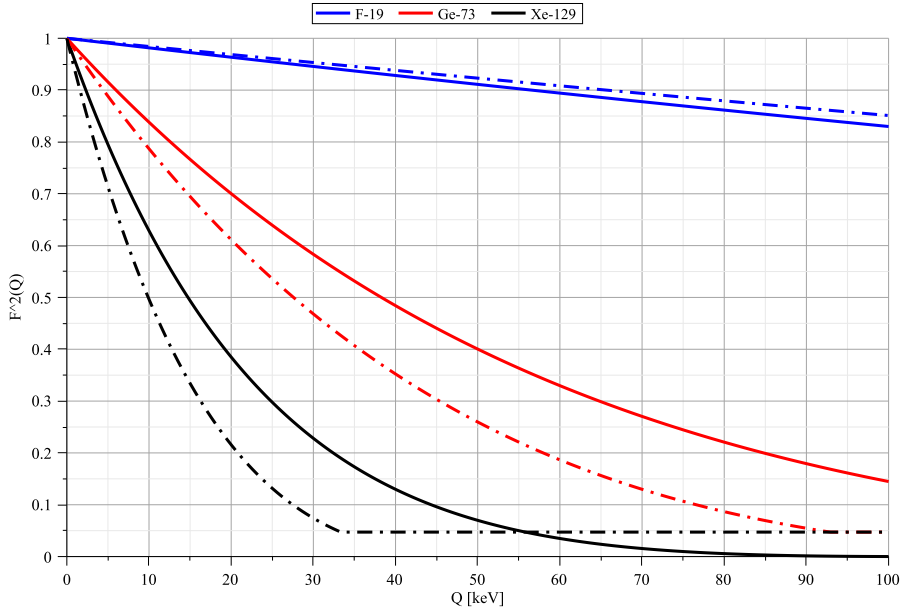


Figure 5: Nuclear form factors of the ^{19}F (top blue), the ^{73}Ge (middle red), and the ^{129}Xe (bottom black) nuclei as functions of the recoil energy. The solid and dash-dotted curves indicate the form factors corresponding to the SI and SD cross sections adopted in our simulation package, respectively [12].

seems to indicate that, the kinetic behavior of (light target nuclei like) ^{19}F scattered by (100-GeV) halo WIMPs could be approximated by scattering by (100-GeV) WIMPs moving with monotonically the root-mean-square velocity.

However, in the middle- and bottom-right frames of Figs. 4, the recoil-angle distributions of the accumulated and the average recoil energies of the ^{19}F target (scattered by 100-GeV WIMPs), namely $Q(\theta_{\text{N}_R, \chi_{\text{in}}}) f_{\text{N}_R, \chi_{\text{in}}, \theta}(\theta_{\text{N}_R, \chi_{\text{in}}})$ and $Q(\theta_{\text{N}_R, \chi_{\text{in}}})$, respectively, indicate that, although the recoil-angle distributions of the recoil energy of (light nuclei like) ^{19}F scattered by (100-GeV) WIMPs could be approximated by the (dash-dotted red) average-kinetic-energy curve (within the 1σ statistical uncertainties), discrepancies between the theoretical expectations and the (black) simulation histograms could already be observed around the most-energetic and in the large-recoil-angle ranges, respectively⁷.

3.2 Target dependence of the angular recoil-direction/energy distributions

In Sec. 3.1, it has been found that the kinetic behavior (the recoil-angle distributions of the recoil direction and the accumulated/average recoil energies) of (light target nuclei like) ^{19}F scattered by (100-GeV) halo WIMPs might be approximated by scattering by (100-GeV) WIMPs moving with monotonically the root-mean-square velocity/average kinetic energy (within the 1σ statistical uncertainties).

On one hand, as shown in Fig. 5, the cross section (nuclear form factor) suppression of

⁷Most (black) simulation histograms here are higher than the theoretical expectations. In Ref. [13], we will show that the average velocity of the (100-GeV) WIMPs scattering off (light nuclei like) ^{19}F is indeed a bit higher than that of the entire incident halo WIMPs.

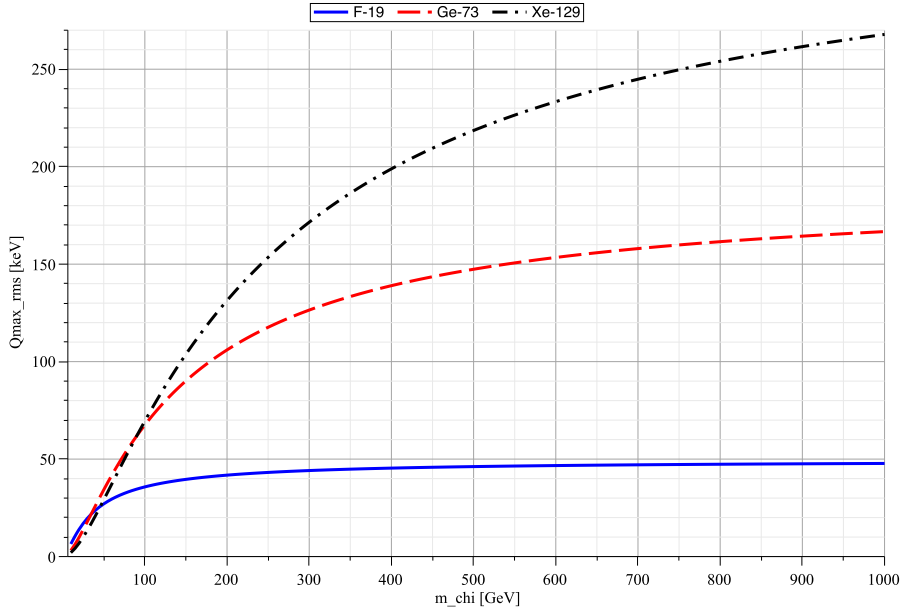


Figure 6: The WIMP–mass dependence of the maximum of the recoil energy, $Q_{\max,\text{rms}}$, given by Eq. (10). Three frequently used target nuclei: ^{19}F (bottom solid blue), ^{73}Ge (middle dashed red), and ^{129}Xe (top dash–dotted black) have been considered.

(light nuclei like) ^{19}F is (relatively) pretty weak. On the other hand, in Fig. 6, the WIMP–mass dependence of the maximum (prefactor) of the recoil energy Q given by Eq. (4) with the root–mean–square velocity as the common velocity of incident WIMPs:

$$Q_{\max,\text{rms}} = \left(\frac{2m_{\text{r},\text{N}}^2}{m_{\text{N}}} \right) v_{\text{rms,Lab}}^2, \quad (10)$$

shows that the maximal recoil energy transferred by WIMPs increases basically with the increased mass of the target nucleus (and/or that of incident WIMPs). Hence, in this subsection, we consider ^{73}Ge and ^{129}Xe as one middle–mass and one heavy target nuclei in our simulations, in order to investigate the target dependence of the recoil–angle distributions of the recoil direction (flux)/energy of scattered target nuclei.

In Figs. 7 and 8, we show the angular distributions and the corresponding recoil–angle dependences of the recoil direction (flux) and the accumulated/average recoil energies of ^{73}Ge and ^{129}Xe target nuclei (scattered by 100–GeV halo WIMPs)⁸. Firstly, it can be found from the top–two rows of two figures that the most frequent/energetic recoil directions (angles) of both nuclei do not appear around the $+\mathbf{Z}_{\chi_{\text{in}}}$ –axis at all, but around the recoil angles of $\theta_{\text{N}_{\text{R}},\chi_{\text{in}}} \simeq 27.5^\circ$ and $\theta_{\text{N}_{\text{R}},\chi_{\text{in}}} \simeq 45^\circ$ for ^{73}Ge and the recoil angles of $\theta_{\text{N}_{\text{R}},\chi_{\text{in}}} \simeq 20^\circ$ and $\theta_{\text{N}_{\text{R}},\chi_{\text{in}}} \simeq 35^\circ$ for ^{129}Xe , respectively. This indicates clearly that, due to the (much) strong(er) cross section (nuclear form factor) suppressions on high recoil energies and thus large recoil angles, the heavier the mass of our target nucleus, the smaller the most–frequent/energetic recoil angles.

Secondly, the right columns of Figs. 7 and 8 show that the kinetic behaviors of both target nuclei (scattered by 100–GeV halo WIMPs) could *not* be approximated by the (dash–dotted red) average–kinetic–energy curve any more: for (middle–mass target nuclei like) ^{73}Ge , the (black)

⁸Interested readers can click each plot in Figs. 4, 7, and 8 to open the corresponding webpage of the animated demonstration with varying target nuclei.

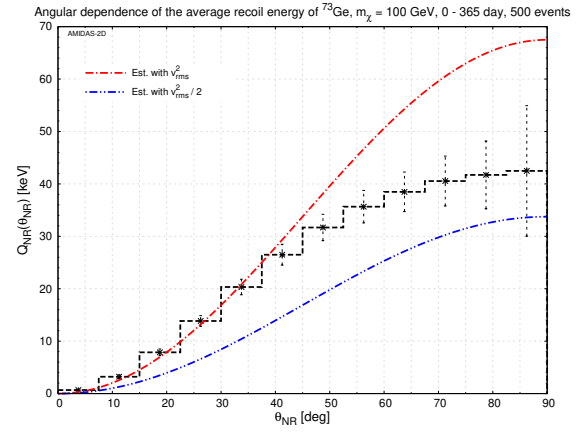
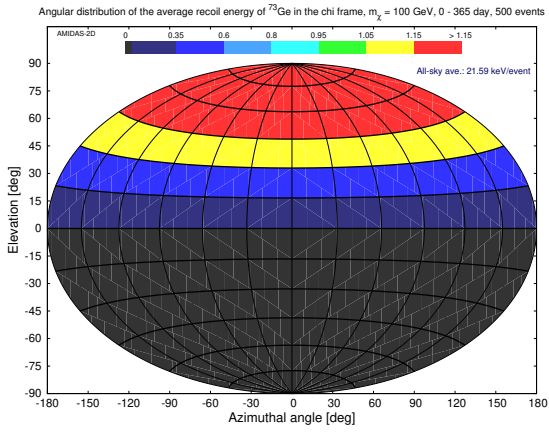
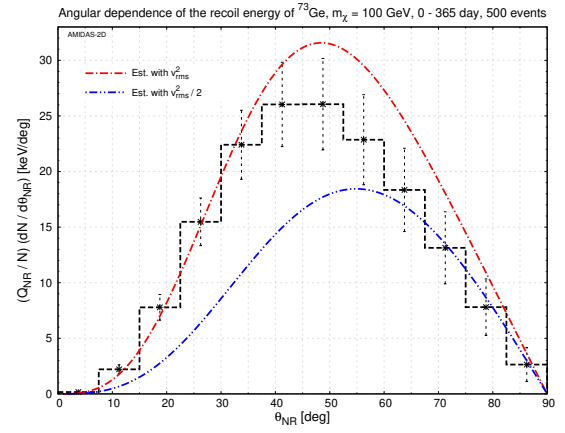
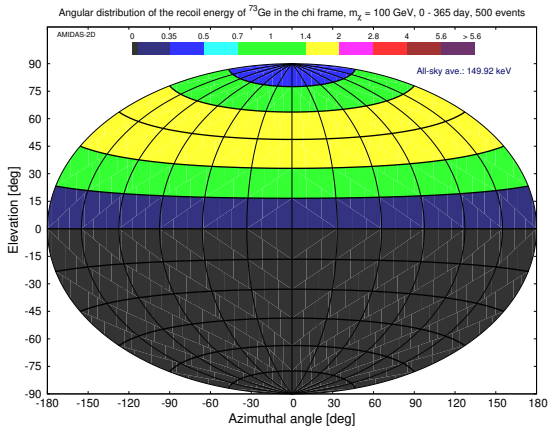
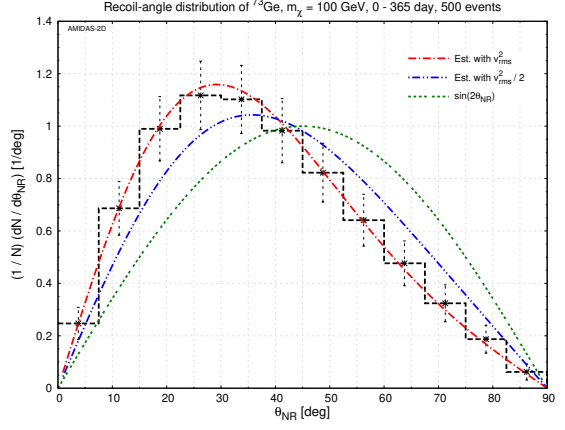
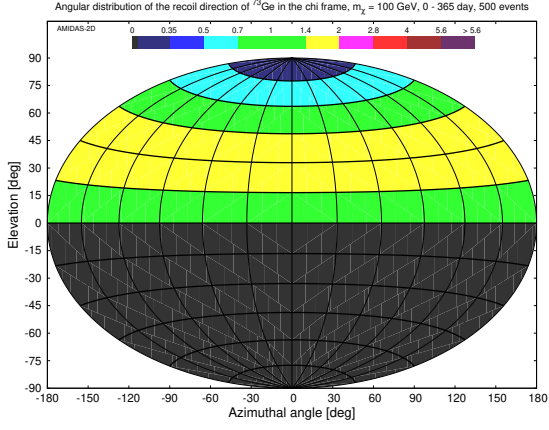


Figure 7: As in Figs. 4, except that a middle-mass nucleus ^{73}Ge has been considered as our target.

simulated histograms match the average-kinetic-energy curve only in the small recoil angle range and move towards the (dash-double-dotted blue) half-average-kinetic-energy curve in the large recoil angle range, whereas, with the increased nuclear mass, for (heavy target nuclei like) ^{129}Xe , the histograms move to approximately between the average- and the half-average-kinetic-energy curves or even closer to the latter in the large recoil angle range.

It is understandable that, once all incident WIMPs move (unrealistically) with the (higher)

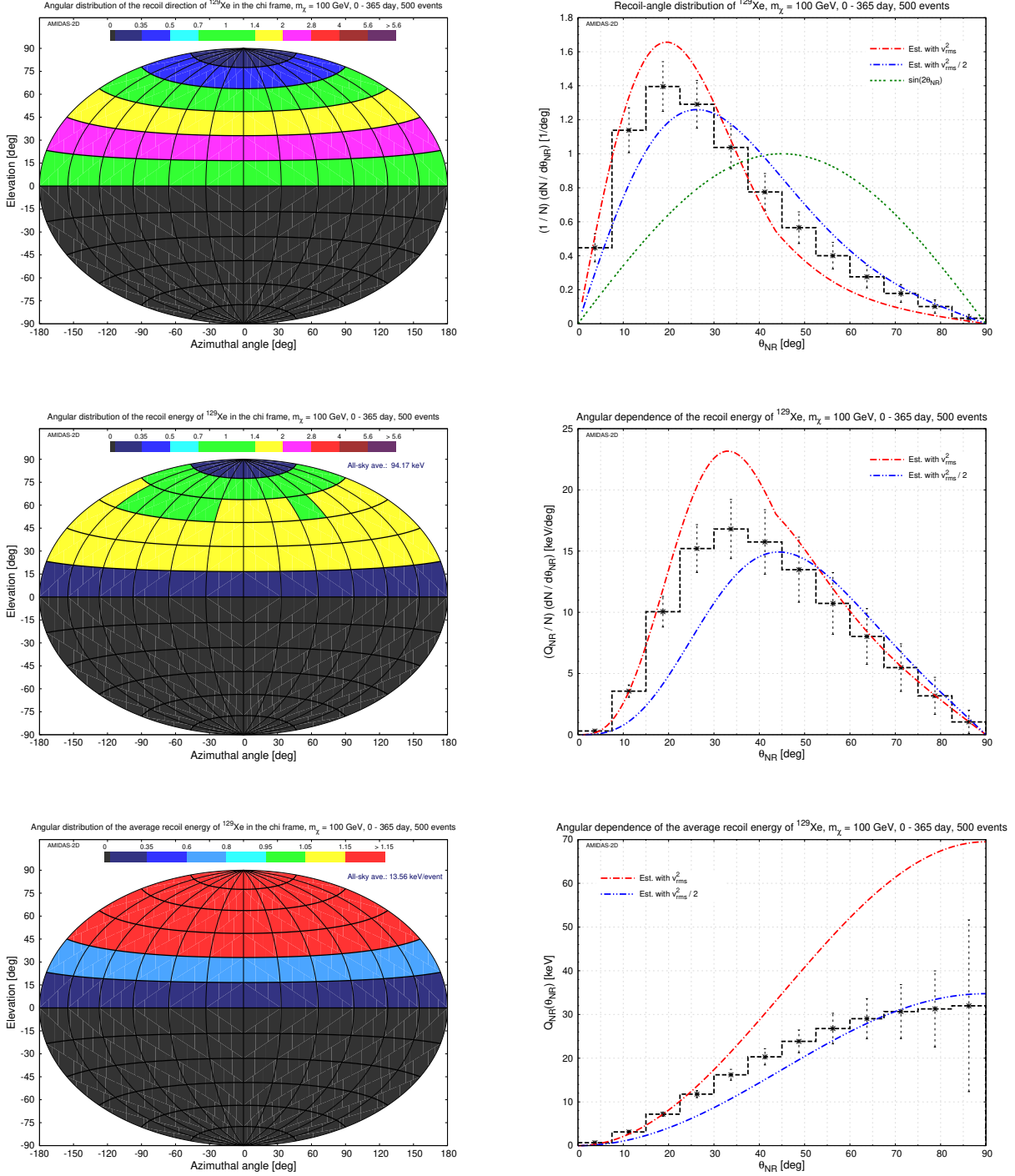


Figure 8: As in Figs. 4 and 7, except that a heavy nucleus ^{129}Xe has been considered as our target.

common root-mean-square velocity $v_{\text{rms,Lab}}$ (and thus the (larger) average kinetic energy $\langle E_\chi \rangle$), the large recoil angle (the large recoil energy) of the scattered target nuclei would be more strongly suppressed due to the sharply reduced cross section (nuclear form factor); in contrast, in the (unrealistic) case that all incident WIMPs move with (the lower) $v_{\text{rms,Lab}}/\sqrt{2}$ (namely only the half of the average kinetic energy), the suppression on the large recoil angle (but only the half of the recoil energy) would be somehow released. And in the real world, as demonstrated

in Ref. [13], the average and the root-mean-square velocities of the 100-GeV WIMPs scattering off (heavy target nuclei like) ^{73}Ge and ^{129}Xe would be smaller than those of the entire group of WIMPs impinging into the detectors. Thus the recoil-angle distributions of ^{73}Ge and ^{129}Xe shift from the average-kinetic-energy curves to the half-average-kinetic-energy curves. However, for cases of very heavy target nuclei (like ^{183}W) scattered by very heavy (e.g. 200-GeV) WIMPs, due to the very strong suppression on high velocity/kinetic energy WIMPs, the incident velocity of most of the WIMPs scattering off target nuclei would be pretty low and thus could sometimes kick target nuclei with large recoil angles.

Remind that the recoil energy Q appearing in the scattering validation criterion (7) depends on the recoil angle $\theta_{\text{NR},\chi_{\text{in}}}$ by Eq. (4). Although the higher the incident velocity of the (simulated) incoming WIMP and/or the larger the recoil angle $\theta_{\text{NR},\chi_{\text{in}}}$, the larger the recoil energy, which could be transferred to the scattered target nucleus, the key point is, as shown in Fig. 5, the larger the recoil energy and/or the heavier the mass of the scattered target nucleus, the stronger the cross section (nuclear form factor) suppression. Hence, the heavier the mass of the target nucleus, the less possible that WIMPs with high incident velocities scatter off the nuclei with large recoil angles, as demonstrated in Figs. 4, 7, and 8.

Finally, the angular and recoil-angle distributions of the average recoil energies of two nuclei in the bottom rows of Figs. 7 and 8 show that, although the maximal transferable recoil energies by 100-GeV WIMPs moving with the root-mean-square velocity are approximately equal for ^{73}Ge and ^{129}Xe (see also Fig. 6), due to its much stronger cross section (nuclear form factor) suppression, the average recoil energy of the ^{129}Xe nucleus is clearly smaller than that of the ^{73}Ge nucleus.

3.3 WIMP-mass dependence of the angular recoil-direction/energy distributions

Following the previous Sec. 3.2, in this subsection, we turn to discuss the WIMP-mass dependence of the angular distributions of the recoil direction/energy of scattered target nuclei.

At first, due to its light nuclear mass, the mass-dependent factor of the recoil energy of the ^{19}F nucleus given by Eq. (4), $2m_{\text{r},\text{N}}^2/m_{\text{N}}$, varies from ~ 10 GeV (for $m_{\chi} = 20$ GeV) to ~ 30 GeV (for $m_{\chi} = 200$ GeV): only ~ 3 times enlarged. Additionally, the nuclear form factor of ^{19}F reduces (relatively) pretty flat (see Fig. 5). The differences of the angular distributions of the recoil direction/energy of the light ^{19}F nucleus scattered by light (20-GeV) WIMPs or by heavier (200-GeV) WIMPs shown in Figs. 9 and 10 would be pretty small, but all characteristics discussed in detail below would already be observable.

In contrast, due to their much larger enlargements of the mass-dependent factor of the recoil energy: varies from ~ 7 GeV to ~ 76 GeV (~ 11 times enlarged) for the ^{73}Ge target and varies from ~ 5 GeV to ~ 94 GeV (~ 19 times enlarged) for the ^{129}Xe target, as well as their much more sharply reduced cross section (nuclear form factor) with the increased recoil energy, the angular recoil-direction/energy distributions of the middle-mass ^{73}Ge nucleus and, in particular, the heavy ^{129}Xe nucleus scattered by 20-GeV and 200-GeV WIMPs presented from Figs. 11 to 14 show a clear WIMP-mass dependence⁹: for a given target nucleus, the larger the WIMP mass, the smaller the most frequent/energetic recoil angles; once the WIMP mass is as heavy as $\mathcal{O}(200 \text{ GeV})$, only a small fraction of incident halo WIMPs (with low incident velocities) could scatter off (heavy target nuclei like) ^{129}Xe with large recoil angles.

⁹Interested readers can click each plot in Figs. 9 to 14 to open the corresponding webpage of the animated demonstration with the varying WIMP mass (for more considered target nuclei).

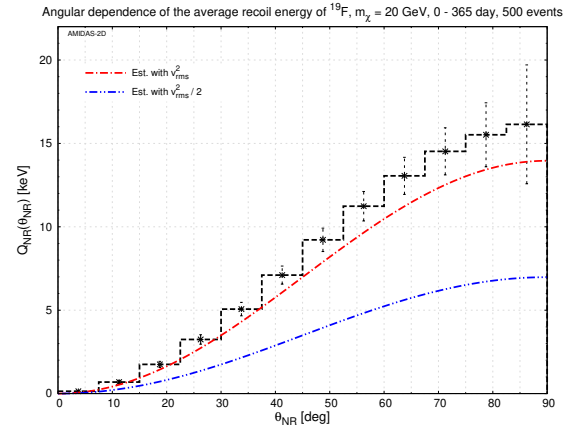
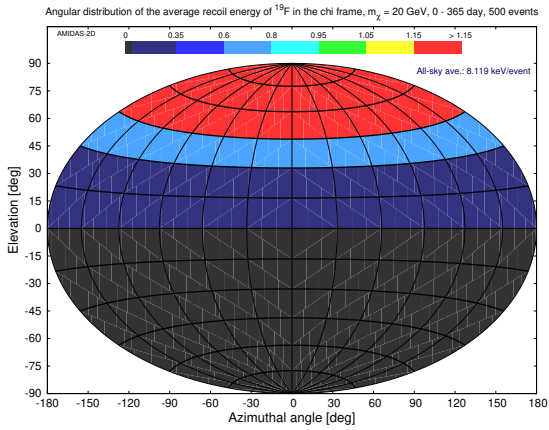
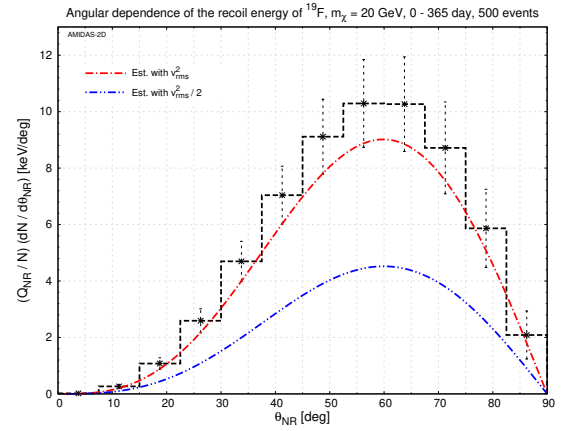
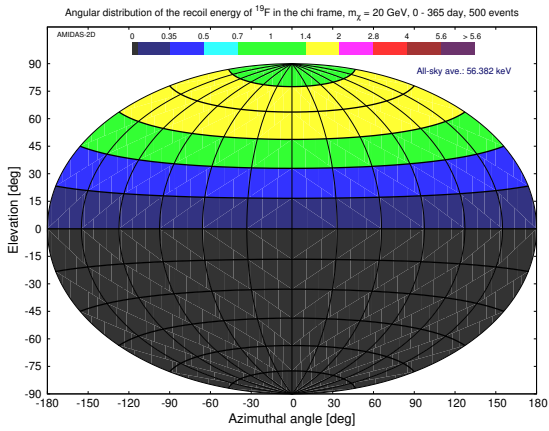
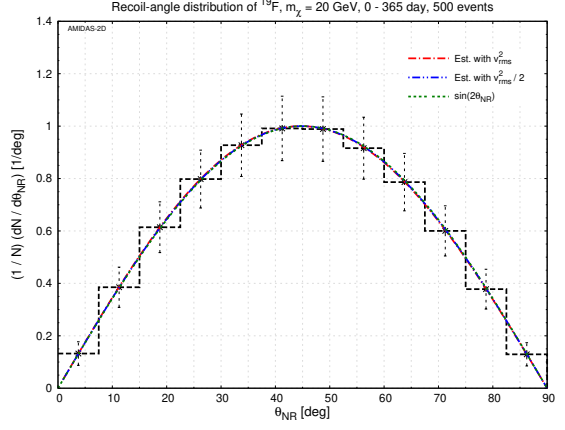
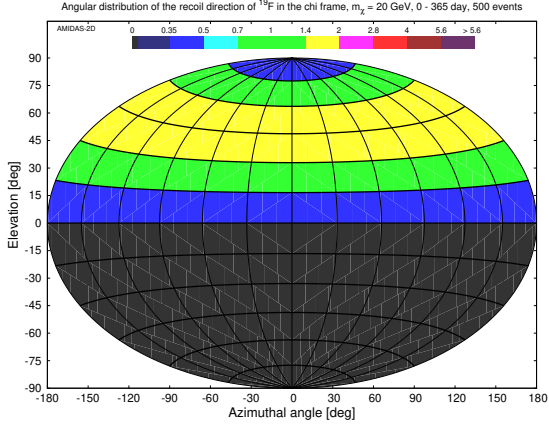


Figure 9: As in Figs. 4: ^{19}F has been considered as the target nucleus, except that the mass of incident WIMPs has been considered as light as $m_\chi = 20$ GeV.

Moreover, the flat recoil-angle distributions of the average recoil energies of the scattered ^{73}Ge and ^{129}Xe nuclei in the high- $\theta_{\text{NR},\chi_{\text{in}}}$ ranges shown in the bottom-right frames of Figs. 12 and 14 would confirm our observation discussed in Sec. 3.2: although the WIMP kinetic energy and thus the maximal theoretically transferable recoil energy (with a given incident velocity) increases rapidly with the increase of the considered WIMP mass (see Fig. 6), the actual increase of the average recoil energy (in particular, in the high- $\theta_{\text{NR},\chi_{\text{in}}}$ range) would strongly be limited,

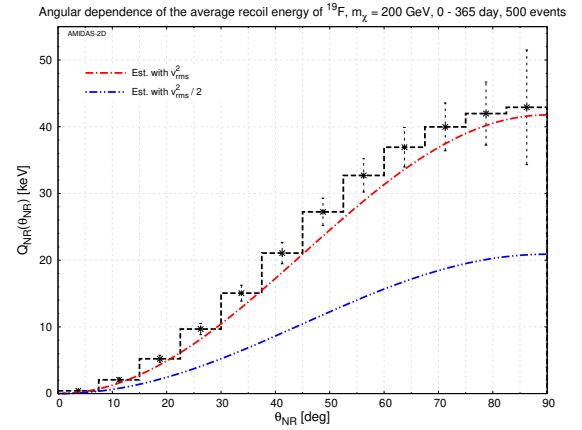
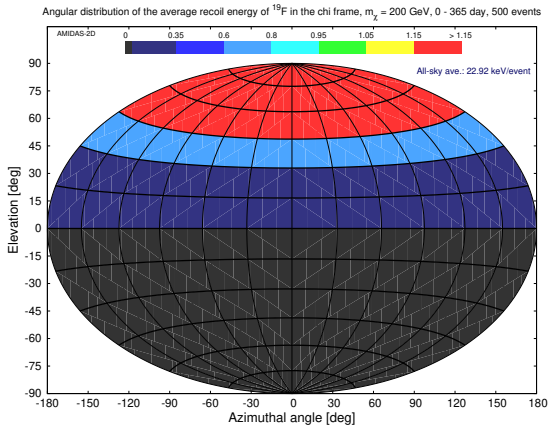
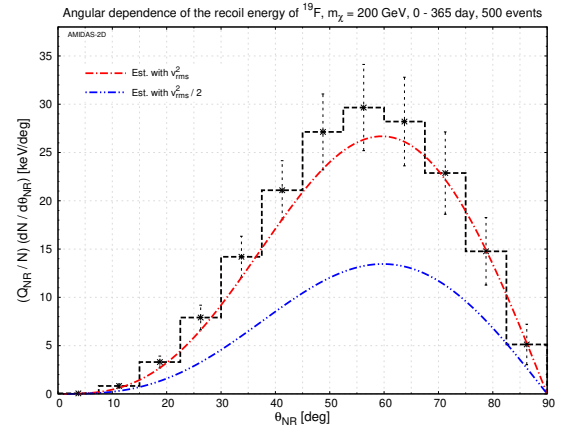
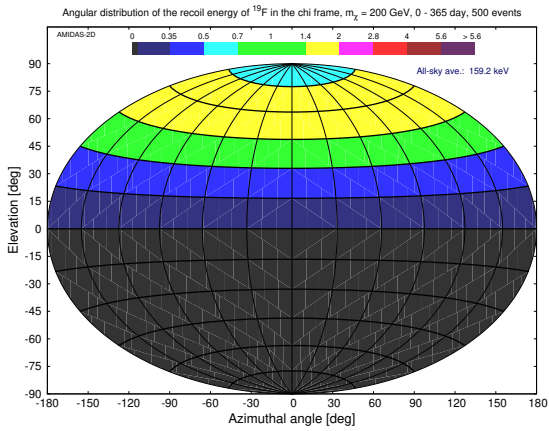
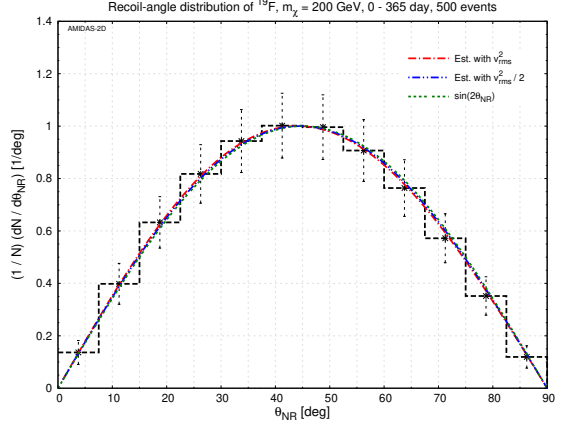
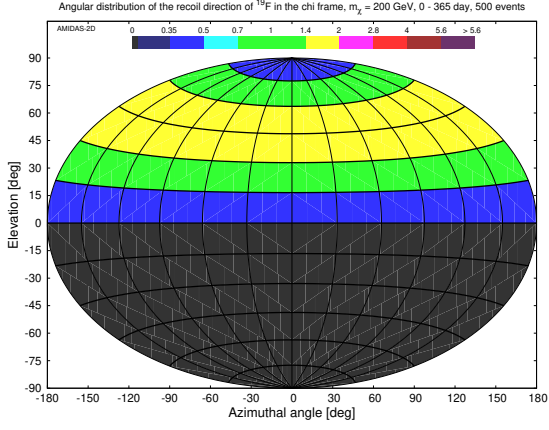


Figure 10: As in Figs. 9 and 4: ^{19}F has been considered as the target nucleus, except that the mass of incident WIMPs has been considered as heavy as $m_\chi = 200$ GeV.

due to, as already emphasized, the cross section (nuclear form factor) suppression.

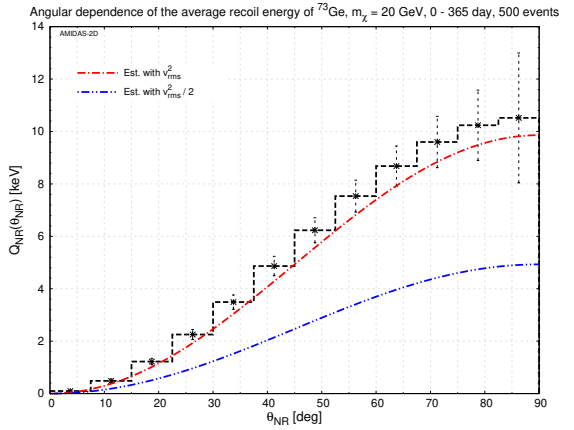
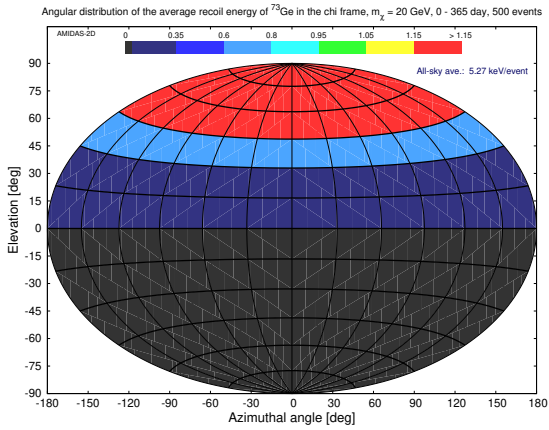
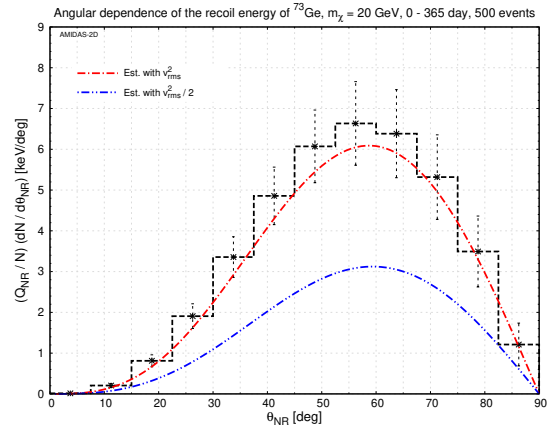
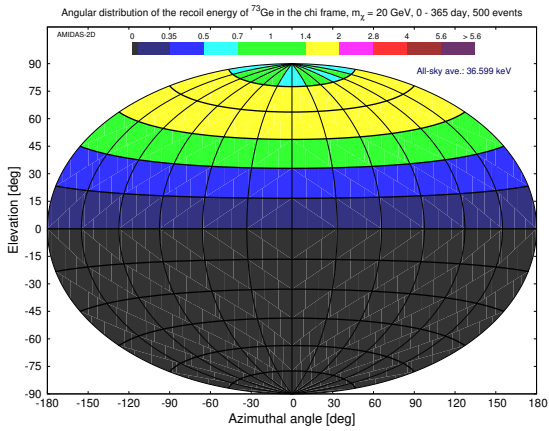
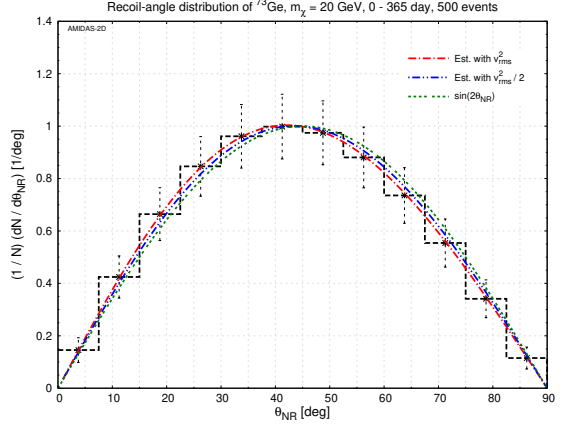
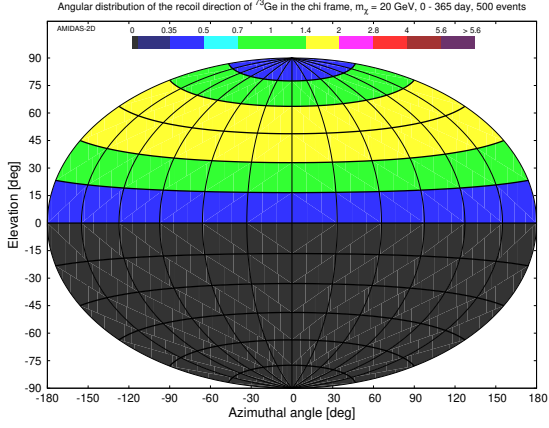


Figure 11: As in Figs. 7: ^{73}Ge has been considered as the target nucleus, except that the mass of incident WIMPs has been considered as light as $m_\chi = 20$ GeV.

3.4 Annual modulation of the angular recoil–direction/energy distributions

Due to the orbital rotation of the Earth around the Sun, the relative velocity of incident halo WIMPs with respect to our laboratory/detector varies annually. Then the flux and the kinetic energy of incident WIMPs as well as the recoil energy of target nuclei scattered by incident

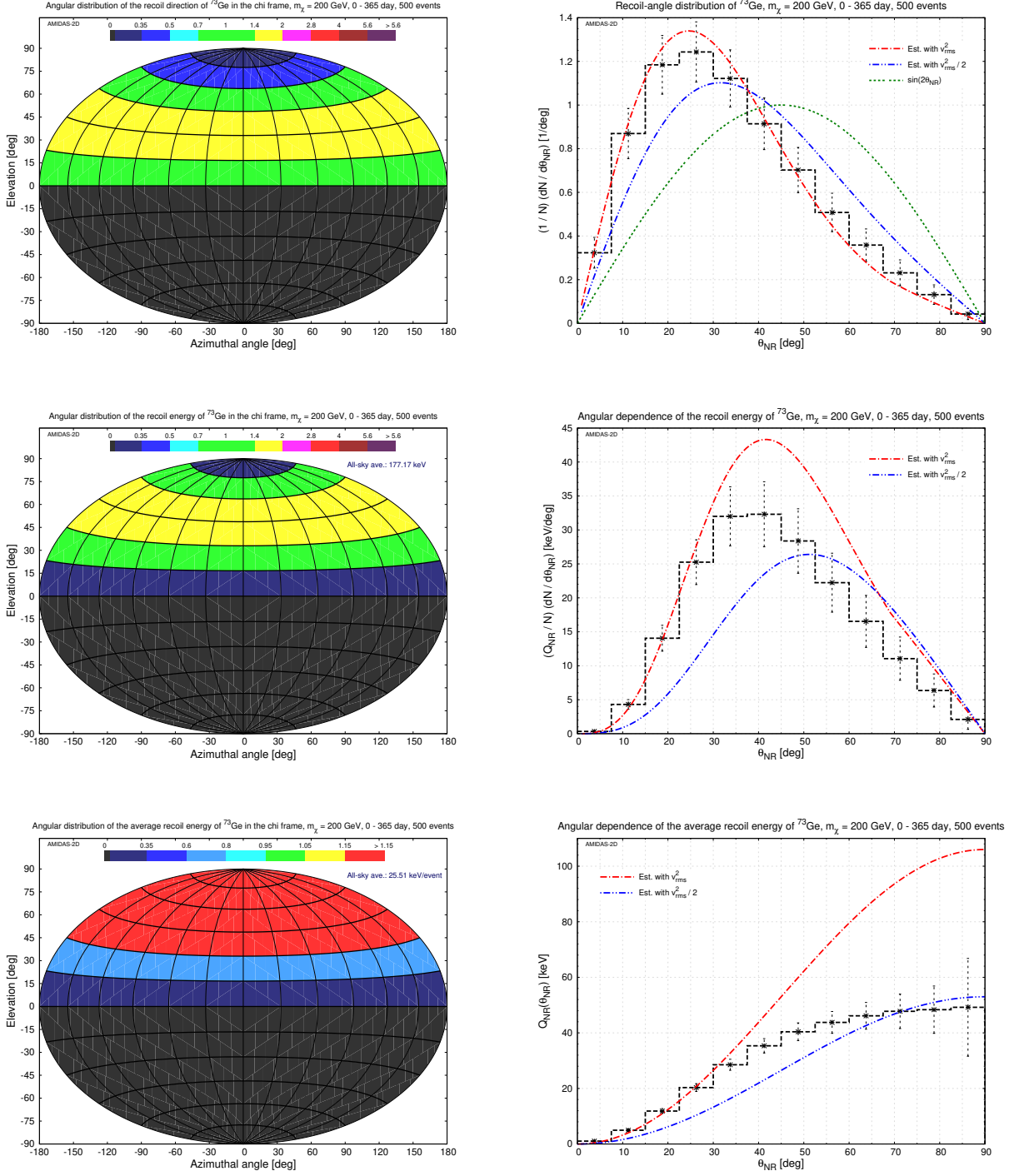


Figure 12: As in Figs. 11 and 7: ^{73}Ge has been considered as the target nucleus, except that the mass of incident WIMPs has been considered as heavy as $m_\chi = 200$ GeV.

WIMPs should in turn vary annually. Hence, in this subsection, we discuss briefly the annual modulation of the angular ($\theta_{N_R, \chi_{in}}$) distributions of the recoil direction (flux) and the accumulated/average recoil energies of WIMP–scattered target nuclei in the incoming–WIMP coordinate system.

In Figs. 15, 16, and 17, we show the recoil–angle distributions of the event number (top), the accumulated (middle) and the average (bottom) recoil energies of three target nuclei scattered

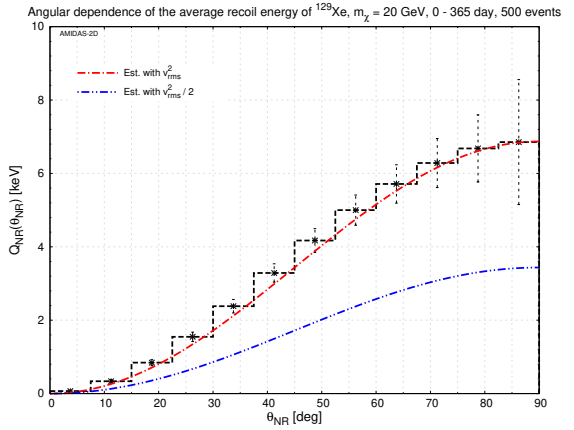
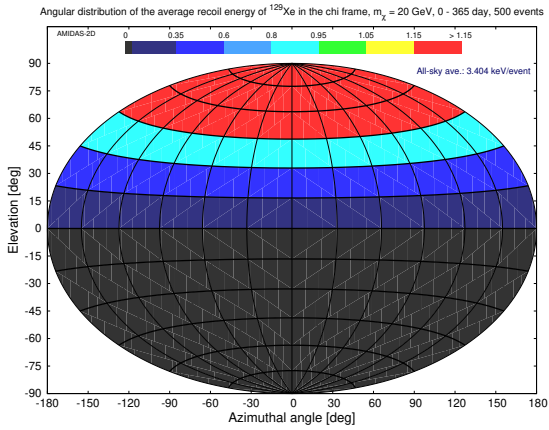
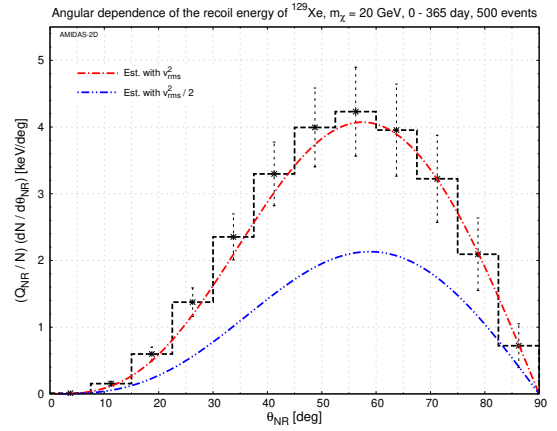
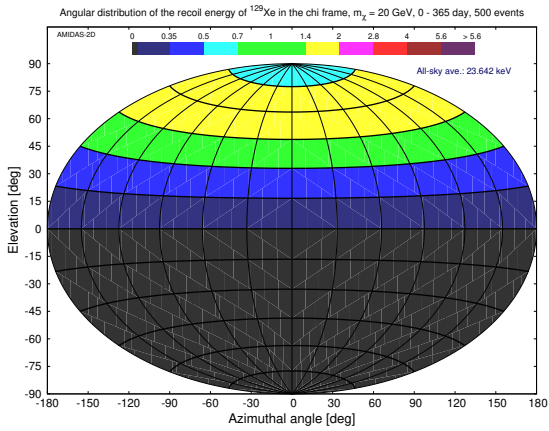
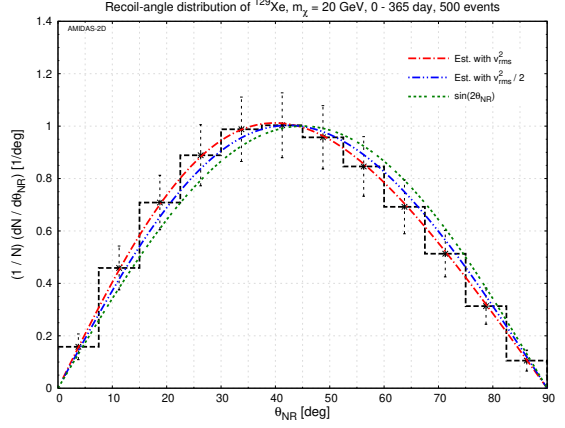
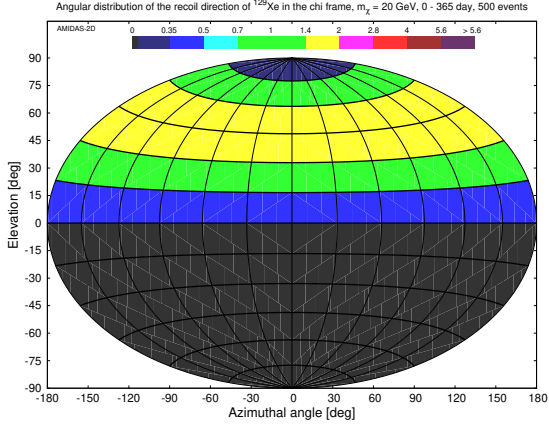


Figure 13: As in Figs. 8: ^{129}Xe has been considered as the target nucleus, except that the mass of incident WIMPs has been considered as light as $m_\chi = 20$ GeV.

by 100-GeV WIMPs with 500 accepted events on average in each 60-day observation period of four *advanced* seasons [10]¹⁰.

Although, considering the large (1σ) statistical uncertainties, it should practically be very difficult to identify these tiny annual variations with $\mathcal{O}(500)$ or even a few thousands of WIMP

¹⁰Interested readers can click each row in Figs. 15, 16, and 17 to open the webpage of the animated demonstration for the corresponding annual modulation (and for more considered WIMP masses and target nuclei).

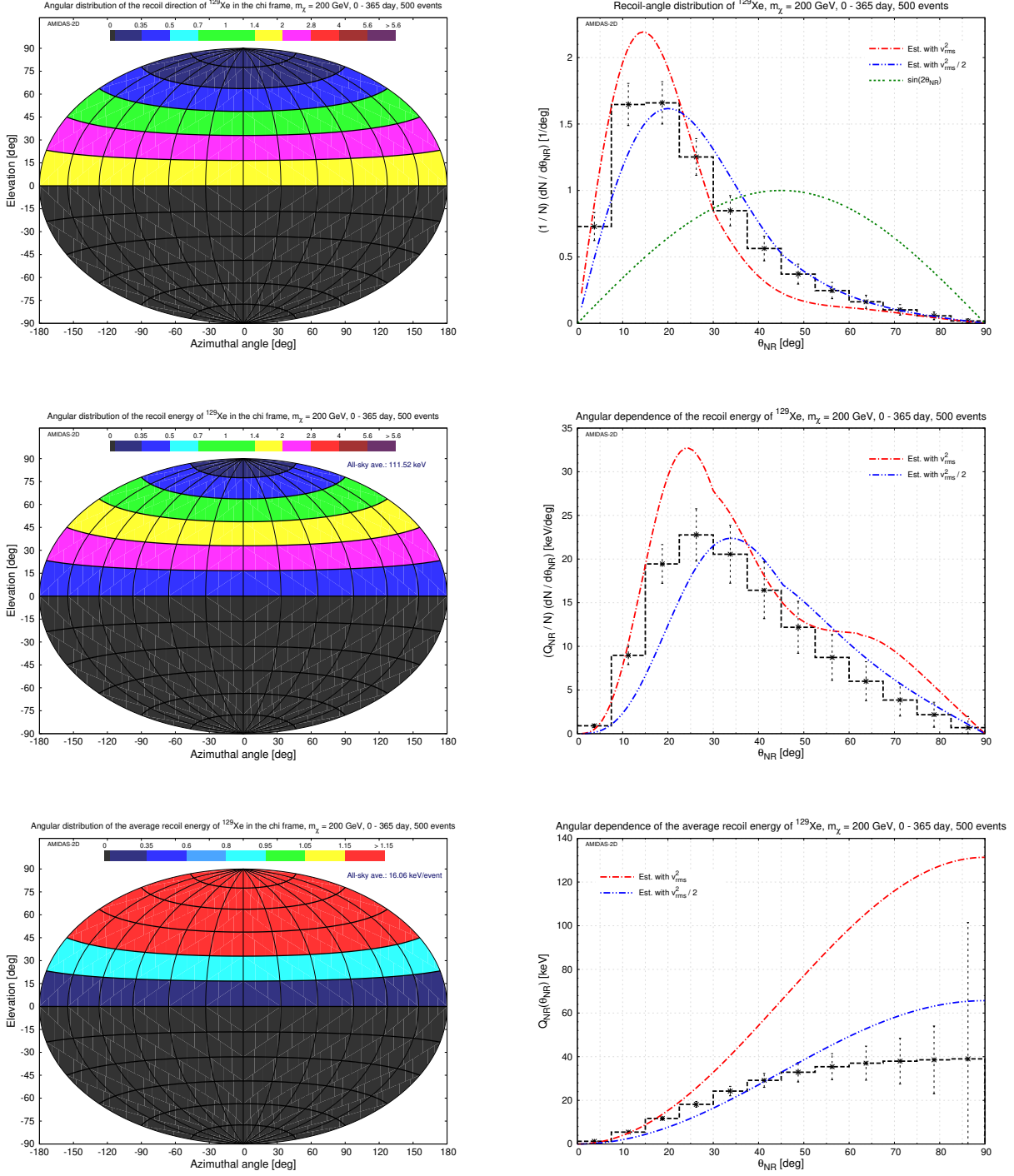


Figure 14: As in Figs. 13 and 8: ^{129}Xe has been considered as the target nucleus, except that the mass of incident WIMPs has been considered as heavy as $m_\chi = 200$ GeV.

scattering events observed in each season (in several consecutive years), it would still be worth to note here that there would indeed be tiny differences between the distributions of the recoil angle as well as those of the accumulated/average recoil energies in different (advanced) seasons: while more scattering WIMPs would have higher (lower) incident velocity in the advanced summer (winter) [13], firstly, more scattered target nuclei would go to smaller (larger) recoil angles in summer (winter); secondly, the accumulated recoil energy in the small (or even all) recoil angles

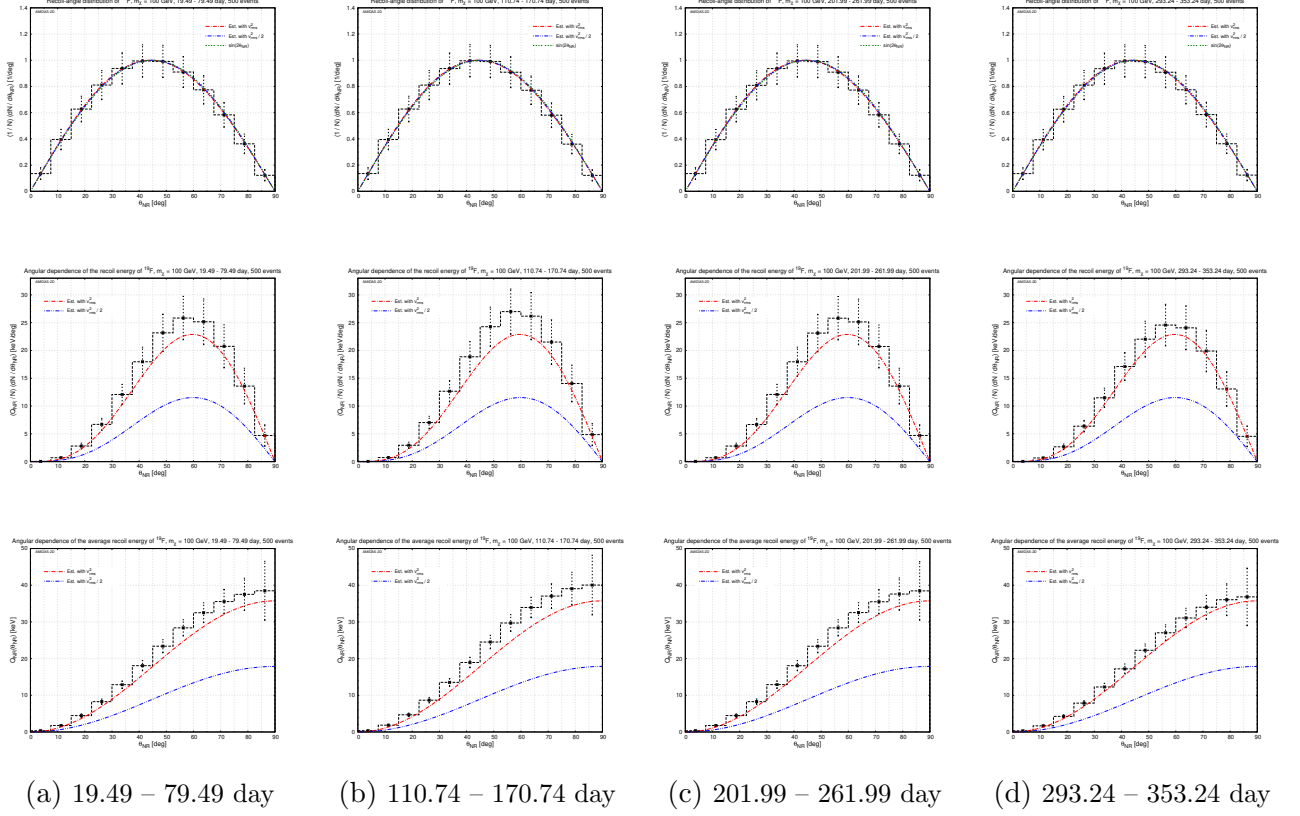


Figure 15: As in the right column of Figs. 4: ^{19}F target nuclei scattered by 100-GeV WIMPs, except that 500 accepted events on average in each 60-day observation period of four *advanced* seasons [10, 12] have been considered.

would be maximal (minimal) in summer (winter); and, finally, the average recoil energy (per event) in all recoil angles would also be maximal (minimal) in summer (winter).

4 Angular distributions of the recoil direction/energy in the laboratory frame

In this section, we move to discuss the angular distributions of the recoil direction (flux) as well as the accumulated and the average recoil energies of scattered target nuclei observed in the laboratory coordinate system. Note that, instead of the angular recoil–direction/energy distributions in the incoming–WIMP coordinate system demonstrated in Sec. 3, this 3-D information on elastic WIMP–nucleus scattering signals could practically be measured in directional direct detection experiments.

In Figs. 18, 19, and 20, we show the angular distributions of the recoil direction (flux) (top), the accumulated (middle) and the average (bottom) recoil energies of the light ^{19}F , the middle-mass ^{73}Ge , and the heavy ^{129}Xe nuclei observed in the laboratory coordinate system of the ANDES laboratory (30.19°S, 69.82°W), which would be the second functional underground laboratory in the Southern Hemisphere [15], in unit of the all-sky average values, respectively. As in Sec. 3, three different masses of incident halo WIMPs: 20 GeV (left), 100 GeV (center), and 200 GeV (right), have been considered¹¹.

¹¹Interested readers can click each row of Figs. 18, 19, and 20 to open the corresponding webpage of the

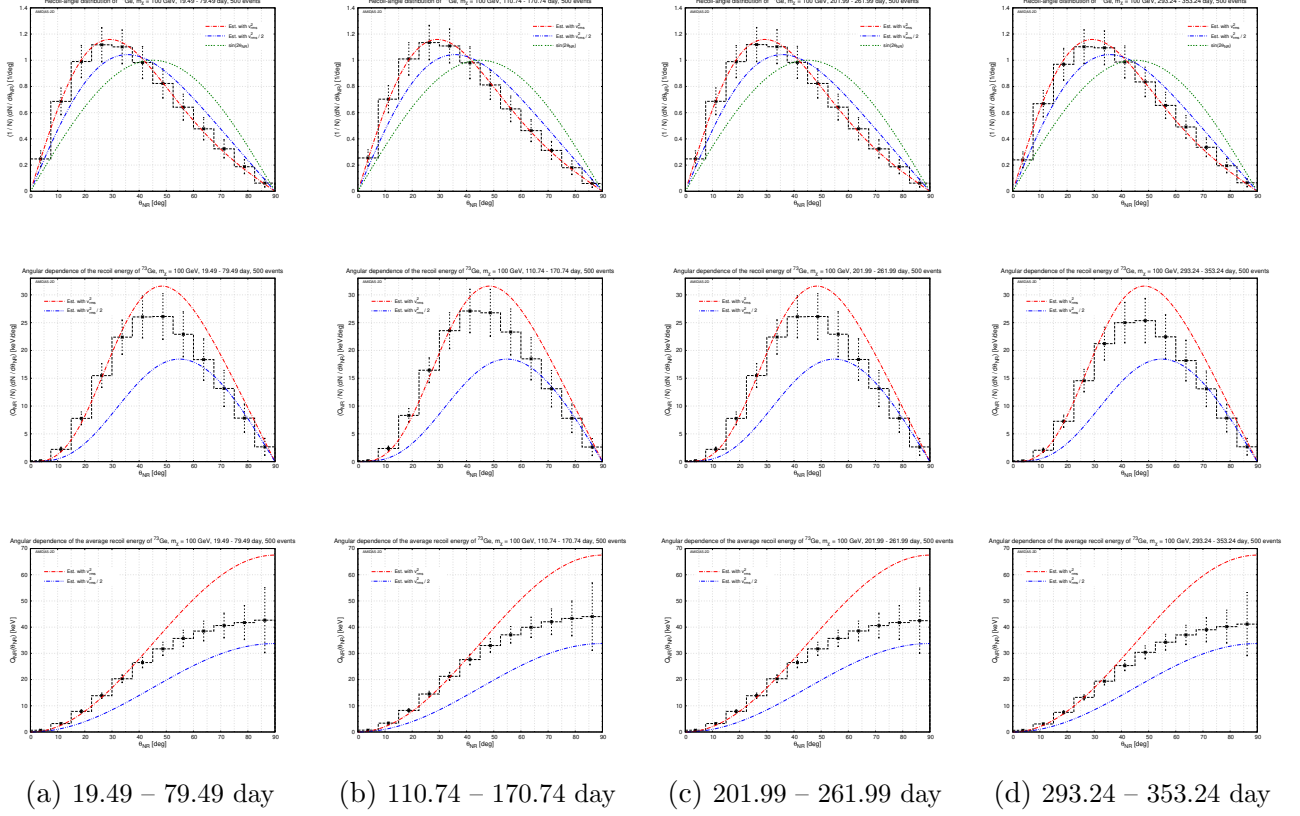


Figure 16: As in Figs. 15, except that a middle-mass nucleus ^{73}Ge has been considered as our target.

First of all, for all three considered target nuclei and three simulated WIMP masses¹², it can be seen directly that the basic distribution patterns of the most frequent/energetic recoil directions (the top and the middle rows) spread approximately symmetrically with respect to the azimuthal angle of 180° .

Moreover, similar to the angular recoil-direction/energy distributions of three considered target nuclei in the incoming-WIMP coordinate system discussed previously, one can find that, firstly, for one given target nucleus, the heavier its mass, the more obvious the (qualitative) differences between the angular distribution patterns simulated with different WIMP masses. This would imply that, qualitatively speaking, the 3-D recoil distribution patterns of heavy target nuclei (e.g. ^{129}Xe) would be more useful for identifying the mass (range) of halo WIMPs. Nevertheless, as shown quantitatively in the right columns of Figs. 9 to 14, the all-sky average values of the accumulated/average recoil energies depend strongly on the simulated WIMP mass as well as on the mass of the target nucleus. This means that the normalization standards of the distribution patterns shown in each (corresponding) row of Figs. 18, 19, and 20 are different. Hence, the measured 3-D information about the angular distributions of the recoil direction (flux)/energy of light nuclei (e.g. ^{19}F) would also be helpful for constraining the mass (range) of halo WIMPs.

animated demonstration with the varying WIMP mass (for more considered target nuclei as well as other underground laboratories). One can also check “Target dependence” for the “animation mode” on the webpage to see the animated demonstration with varying target nuclei.

¹²Currently, we consider only rather heavy WIMP masses of $m_\chi \geq 20$ GeV. For light WIMP masses of $m_\chi \leq 20$ GeV, more detailed investigations are needed and will be announced later.

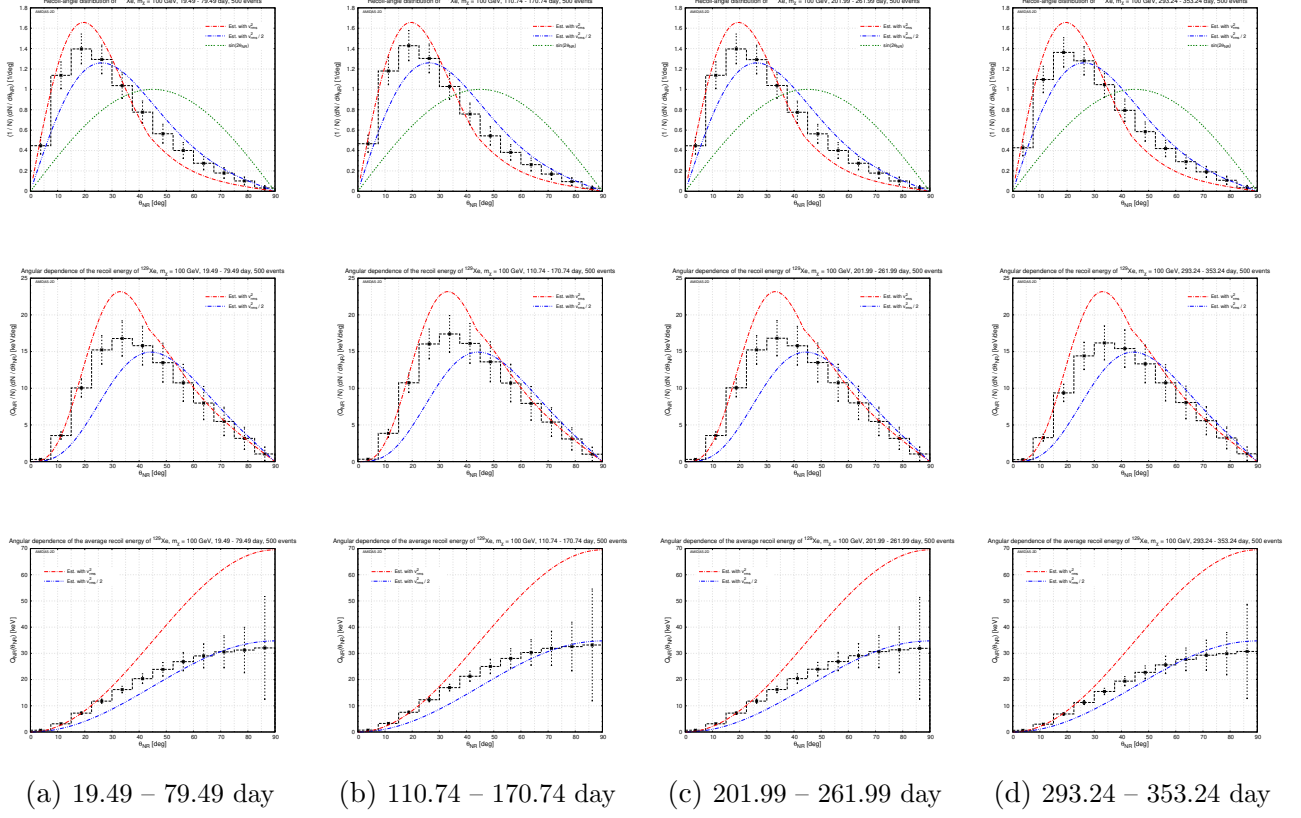


Figure 17: As in Figs. 15 and 16, except that a heavy nucleus ^{129}Xe has been considered as our target.

On the other hand, it could also be clearly observed that, for a given WIMP, the larger the mass difference between two target nuclei (and the larger the considered WIMP mass), the larger the differences between their angular distribution patterns of the recoil direction/energy. This indicates that, by comparing/combining the angular recoil–direction/energy distributions of different target nuclei, we could pin down the mass (range) of halo WIMPs (more precisely).

5 Angular distributions of the recoil direction/energy in the Equatorial frame

Finally, we present in this section the angular distributions of the recoil direction (flux) as well as the accumulated and the average recoil energies of scattered target nuclei observed in the Equatorial coordinate system. Note that, by definition, the Equatorial coordinate system is laboratory/location independent [10]. Hence, considering the very low theoretically estimated event rate, combining and analyzing WIMP scattering events off the same target nucleus provided however from different underground laboratories in the Equatorial coordinate system would be practically a very useful strategy.

In Figs. 21, 22, and 23, we show the angular distributions of the recoil direction (flux) (top), the accumulated (middle) and the average (bottom) recoil energies of the light ^{19}F , the middle-mass ^{73}Ge , and the heavy ^{129}Xe nuclei observed in the Equatorial coordinate system in unit of the all-sky average values. As in Secs. 3 and 4, three different masses of incident halo WIMPs:

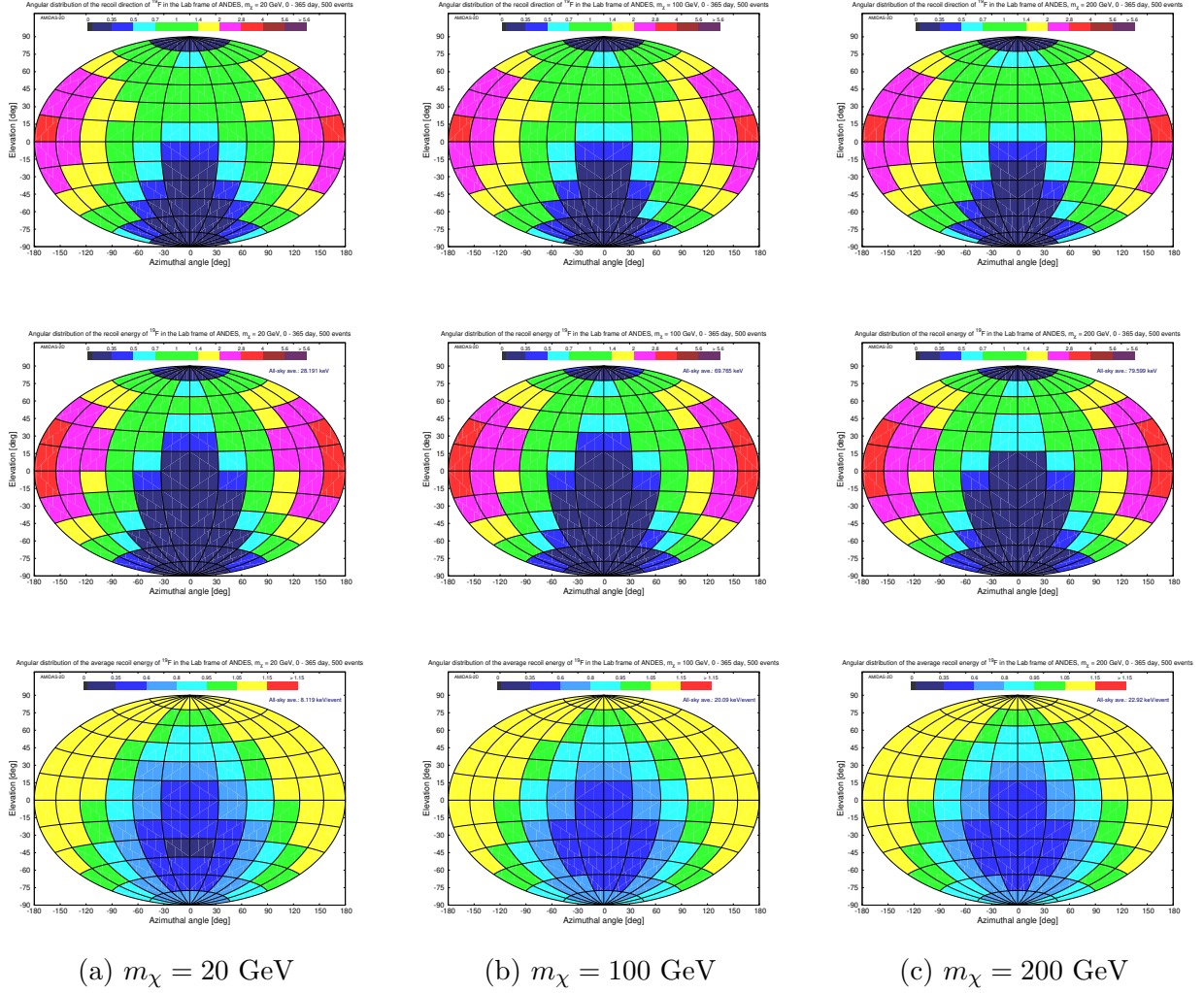


Figure 18: The angular distributions of the recoil direction (flux) (top), the accumulated (middle) and the average (bottom) recoil energies of ^{19}F observed in the laboratory coordinate system of the ANDES laboratory (30.19°S , 69.82°W) [15] in unit of the all-sky average values. The masses of incident WIMPs have been set as $m_\chi = 20 \text{ GeV}$ (left), 100 GeV (center), and 200 GeV (right), respectively. Other simulation setup and notations are the same as in Figs. 9, 4, and 10.

20 GeV (left), 100 GeV (center), and 200 GeV (right), have been considered¹³. The dark-green star in each plot indicates the theoretical main direction of incident WIMPs in the Equatorial coordinate system: [16]: 42.00°S , 50.70°W .

At first, similar to the angular distributions of the recoil direction/energy of three considered target nuclei in the laboratory coordinate system presented in Sec. 4, one can find that, the heavier the mass of one given target nucleus or the larger the mass difference between two target nuclei (and the larger the simulated WIMP mass), the more obvious the pattern differences between the angular recoil-direction/energy distributions of the scattered target nucleus with different WIMP masses or between those of different target nuclei. Hence, by combining and/or

¹³Interested readers can click each row in Figs. 21, 22, and 23 to open the corresponding webpage of the animated demonstration with the varying WIMP mass (for more considered target nuclei). One can also check “Target dependence” for the “animation mode” on the webpage to see the animated demonstration with varying target nuclei.

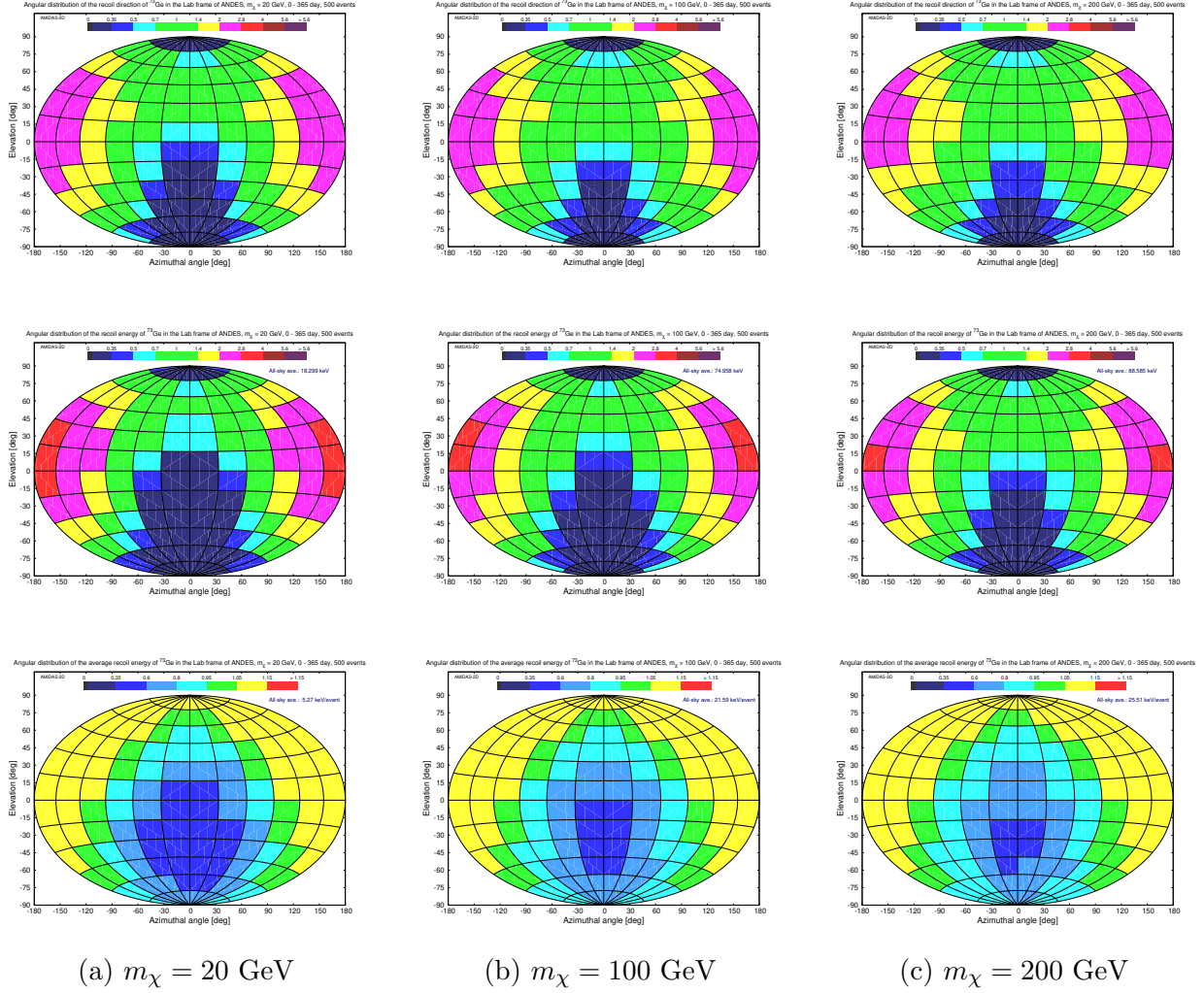


Figure 19: As in Figs. 18, except that a middle-mass nucleus ^{73}Ge has been considered as our target.

comparing the (quantitative) nuclear recoil flux and energy or even only their (qualitative) distribution patterns with the same/different target nuclei (in different underground laboratories) in the Equatorial coordinate system, one could constrain/identify the mass (range) of halo WIMPs.

More importantly, the angular distributions of the recoil direction/energy of all three target nuclei with three considered WIMP masses show clearly the anisotropies. However, unexpectedly, neither the centers of the most frequent recoil directions nor those of the most energetic ones of all simulated target nucleus–WIMP mass combinations (the top and the middle rows) could match the theoretical main direction of the WIMP wind (the dark-green star). Comparing with the small (northwest) deviations of the most frequent and the most energetic incident directions of halo WIMPs presented in Refs. [10, 11], the northerly shifts of (the centers of) the most frequent/energetic recoil directions seem to be much more obvious, and these shifts increase with the increased nuclear and/or WIMP mass. Interestingly, the hot-points of the angular distributions of the “average” recoil energy (the bottom rows) of all simulated target nucleus–WIMP mass combinations seem to be approximately centered around the theoretical main WIMP direction, with nevertheless some small (but observable) target/WIMP–mass dependent pattern differences.

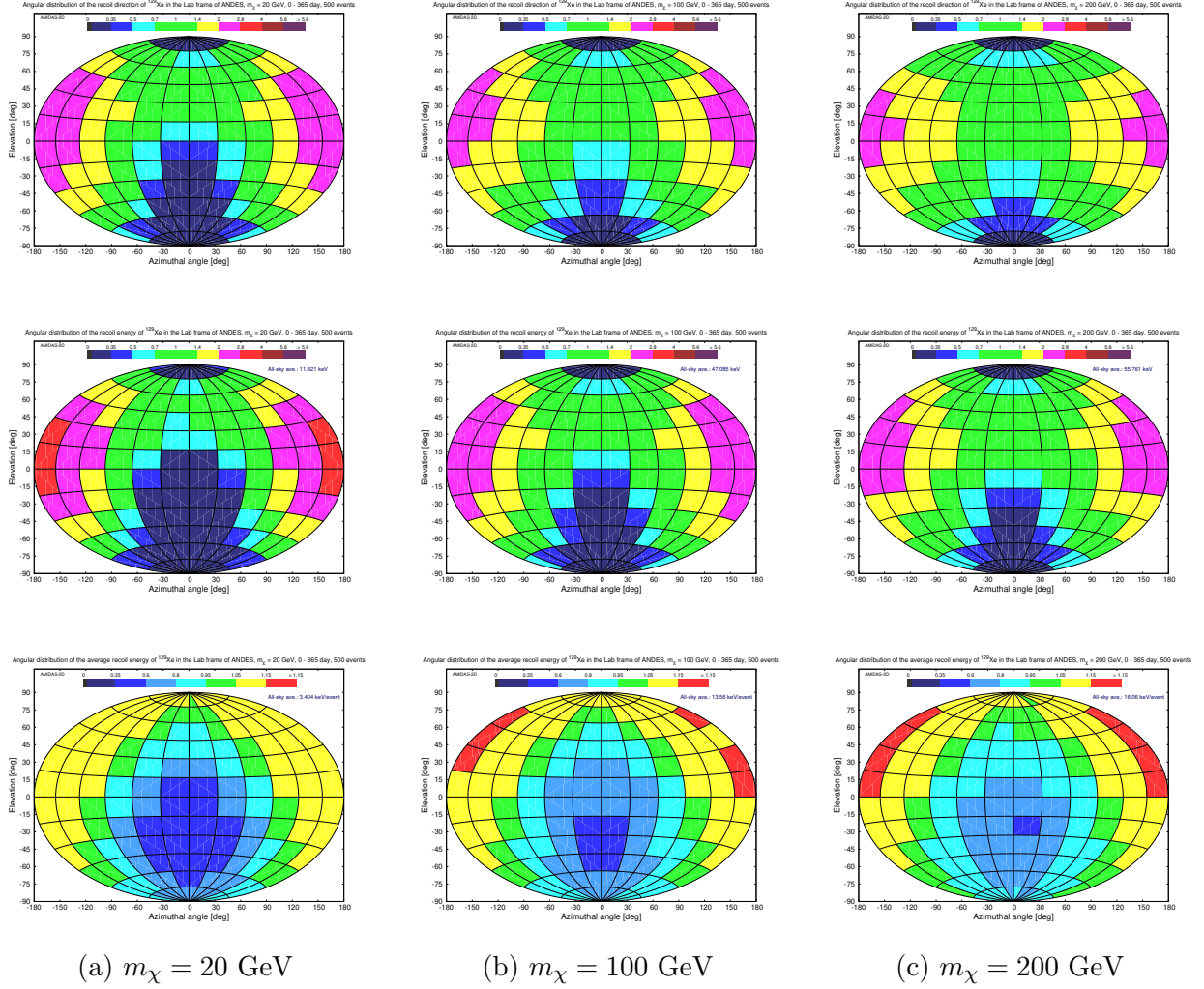


Figure 20: As in Figs. 18 and 19, except that a heavy nucleus ^{129}Xe has been considered as our target.

5.1 Annual modulation of the angular recoil–direction/energy distributions

The original purpose of directional direct Dark Matter detection experiments is to observe the “diurnal” modulated anisotropy (the directionality) of the recoil direction of elastic WIMP–nucleus scattering events [5, 6]. On the other hand, in Refs. [10, 11], we demonstrated that, considering the very low theoretically estimated event rate, it would be equivalent or even better to observe the “annual” modulated anisotropy of the recoil direction of WIMP–scattered target nuclei. Hence, in this subsection, we discuss the annual modulation of the angular distributions of the recoil direction/energy observed in the Equatorial coordinate system.

In Figs. 24, 25, and 26, we show the angular distributions of the recoil direction (flux) (top), the accumulated (middle) and the average (bottom) recoil energies of the light ^{19}F , the middle–mass ^{73}Ge , and the heavy ^{129}Xe nuclei scattered by 100-GeV WIMPs observed in the Equatorial coordinate system in unit of the all–sky average values with 500 accepted events on average in each 60-day observation period of four advanced seasons [10]¹⁴. Besides the dark–green star

¹⁴Interested readers can click each row in Figs. 24 to 27 to open the webpage of the animated demonstration for the corresponding annual modulation (and for more considered WIMP masses and target nuclei).

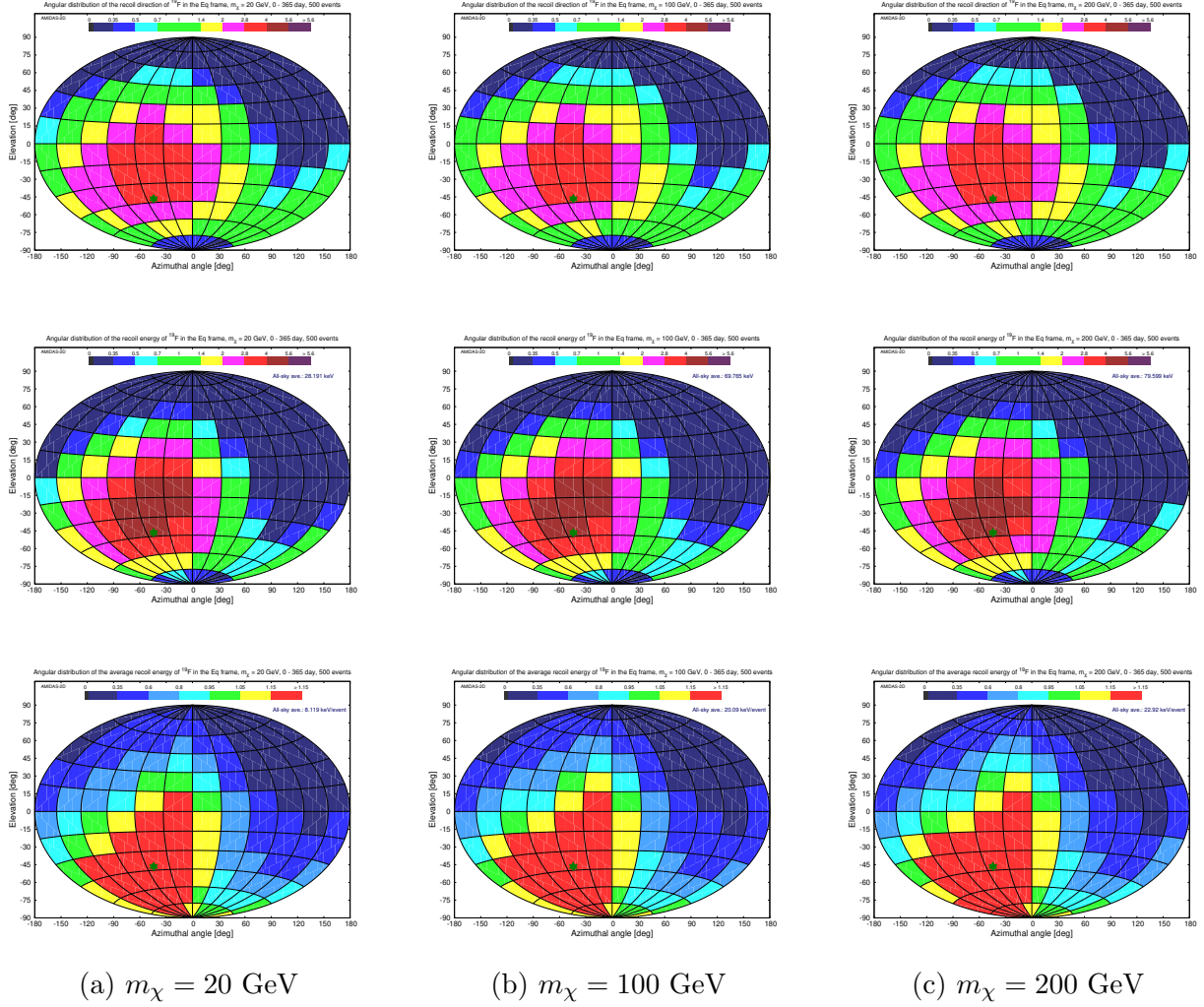


Figure 21: The angular distributions of the recoil direction (flux) (top), the accumulated (middle) and the average (bottom) recoil energies of ^{19}F observed in the Equatorial coordinate system in unit of the all-sky average values. The masses of incident WIMPs have been set as $m_\chi = 20 \text{ GeV}$ (left), 100 GeV (center), and 200 GeV (right), respectively. The dark-green star indicates the theoretical main direction of incident WIMPs in the Equatorial coordinate system [16]: 42.00°S , 50.70°W . The simulation setup and notations are the same as in Figs. 18.

indicating the theoretical main direction of the WIMP wind, the blue-yellow point in each plot indicates the opposite direction of the Earth’s velocity relative to the Dark Matter halo on the central date of the observation period [10].

It can be found that, firstly, while the angular distribution patterns of the “average” recoil energy of three considered target nuclei (the bottom rows) show indeed approximately circular clockwise rotations following the instantaneous theoretical main direction of the incident halo WIMPs, the approximate rotation centers of the distribution patterns of the recoil direction and the accumulated recoil energy (the top and the middle rows) would, as observed previously, clearly shift northwesterly.

Moreover, the annual variations of the angular recoil-direction distributions of (middle-mass nuclei like) ^{73}Ge and (heavy nuclei like) ^{129}Xe seem *not* to be circular, but oscillated somehow *latitudinally*. And the shapes of the most frequent/energetic recoil directions seem also to be somehow *longitudinally* squeezed; the heavier the nuclear (and/or the WIMP) mass,

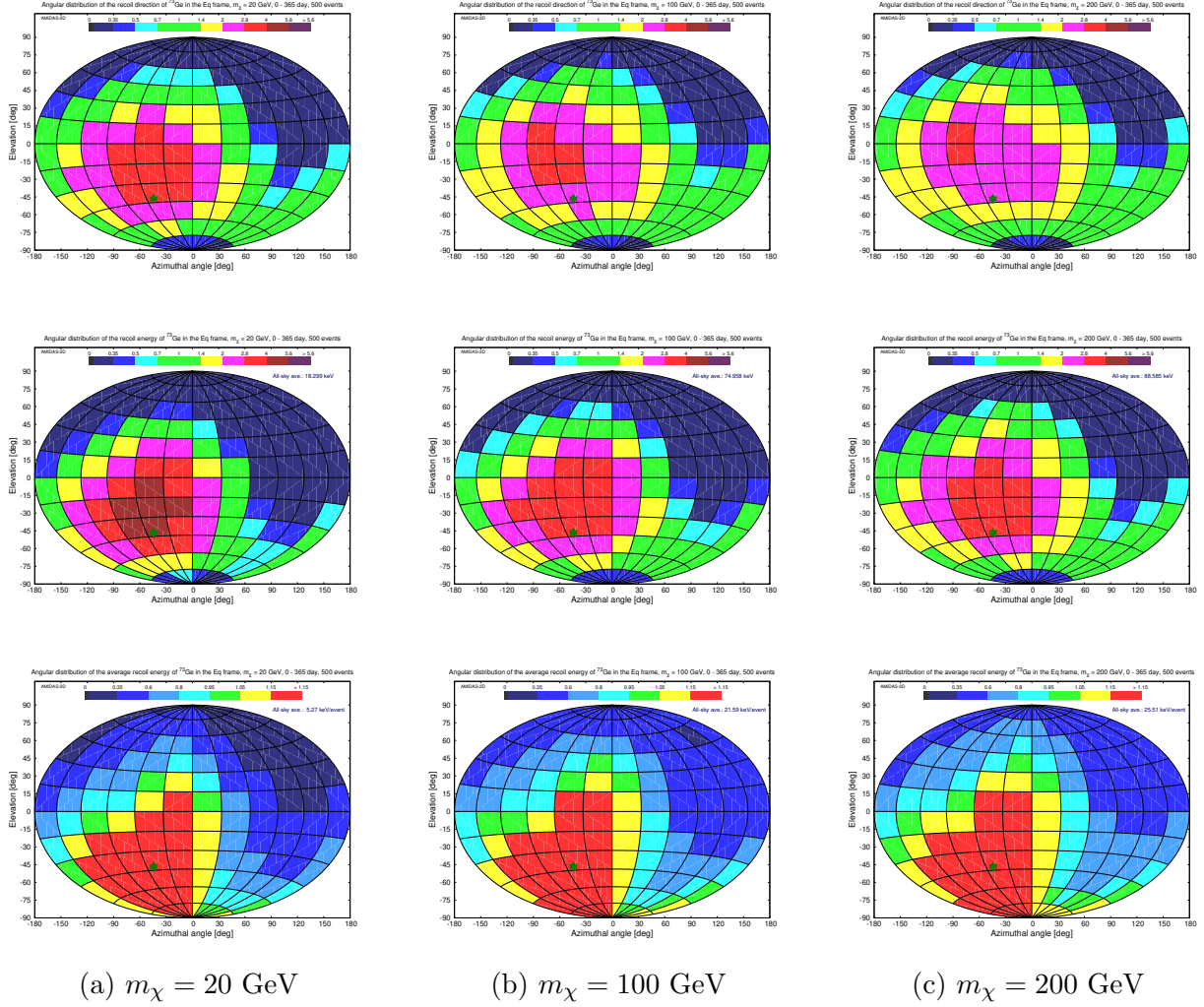


Figure 22: As in Figs. 21, except that a middle-mass nucleus ^{73}Ge has been considered as our target.

the stronger the pattern distortion would be. So far we have no reasonable explanation(s) for this (unexpected) observations.

In Figs. 27, we show the angular distributions of the recoil direction/energy of the heavy ^{129}Xe nuclei with a raised WIMP mass of $m_\chi = 200 \text{ GeV}$, as a demonstration of the WIMP-mass dependence of the annual modulation of the angular recoil-direction/energy distributions. The northwesterly shifts of the approximate rotation centers of the distribution patterns of the recoil direction and the accumulated recoil energy as well as the longitudinal squeeze of the most frequent/energetic recoil directions become now more obvious.

6 Summary

In this paper, as the second part of the third step of our development of data analysis procedures for using and/or combining 3-dimensional information offered by directional direct Dark Matter detection experiments in the future, we investigated the angular distributions of the recoil direction (flux) and the recoil energy of the Monte Carlo simulated WIMP-scattered target nuclei observed in different celestial coordinate systems.

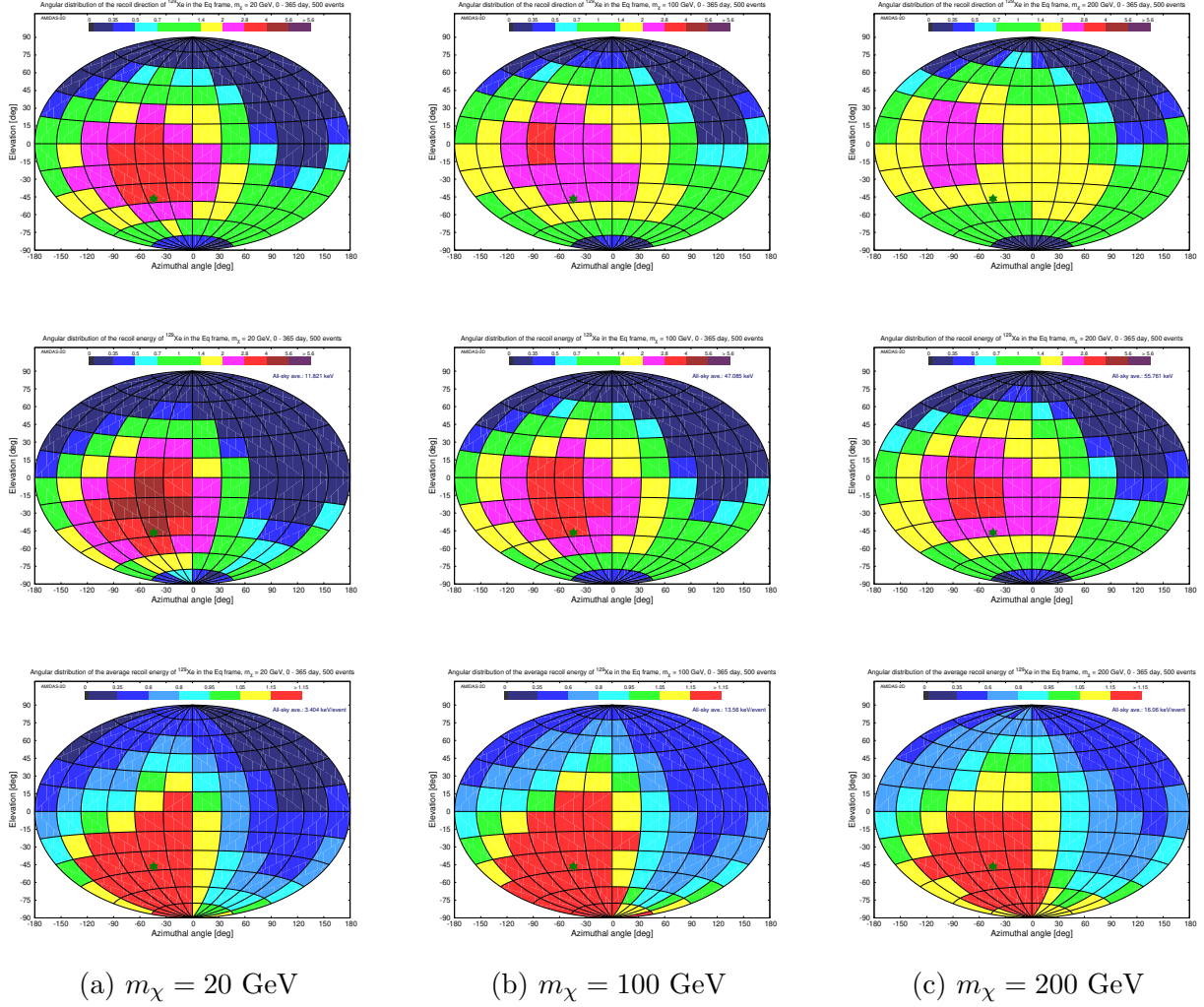


Figure 23: As in Figs. 21 and 22, except that a heavy nucleus ^{129}Xe has been considered as our target.

At first, we demonstrated the angular (all-sky) and the recoil-angle distributions of the recoil direction (flux) as well as the accumulated and the average recoil energies of several frequently used target nuclei in the incoming-WIMP coordinate system. Our simulations showed that, firstly, while the angular distributions of the recoil direction and the accumulated/average recoil energies of all simulated target nucleus-WIMP mass combinations show the azimuthal symmetry in the incoming-WIMP point of view, their recoil-angle distributions have clearly strong target and WIMP-mass dependences. It would be important to emphasize here that the most frequent and the most energetic recoil directions (angles) do *not* appear around the incoming direction of incident WIMPs at all, but have the upper bounds of 45° and 60° , respectively, and reduce strongly with the increased nuclear and/or WIMP mass.

Secondly, the obvious discrepancies between the simulated recoil-angle distributions of the recoil direction/energy and the theoretical expectations for scattering by WIMPs carrying monotonically (the half of) the average kinetic energy indicate clearly that, the kinetic behavior of the subgroup of WIMPs scattering off (specified) target nuclei in an underground detector would be different from that of the entire incident halo WIMPs: due to the sharply reduced cross section (nuclear form factor) with the increased recoil energy, the event numbers as well as the accumulated and the average recoil energies transferred by WIMPs moving with high incident

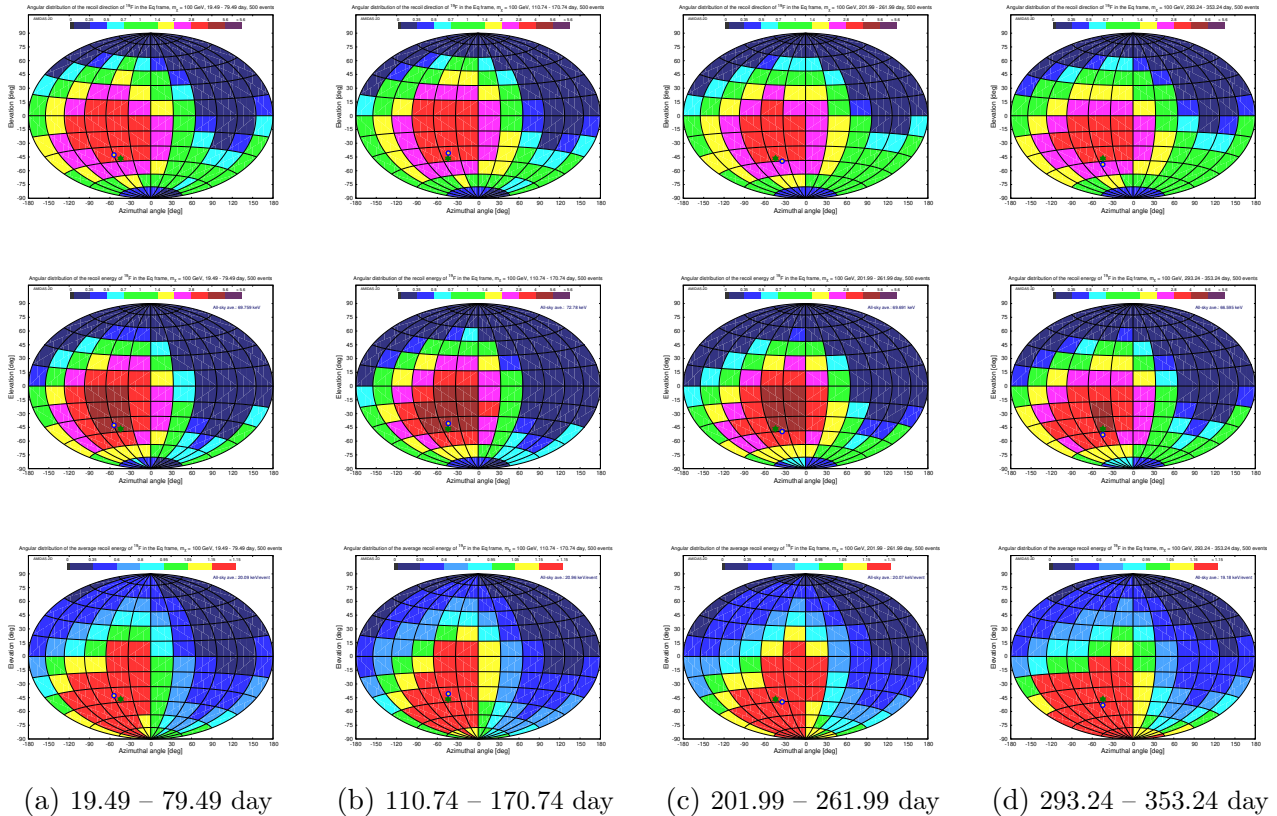


Figure 24: As in Figs. 21(b): ^{19}F target nuclei scattered by 100-GeV WIMPs, except that 500 accepted events on average in each 60-day observation period of four advanced seasons [10, 12] have been considered. Besides the dark-green star indicating the theoretical main direction of the WIMP wind, the blue-yellow point in each plot indicates the opposite direction of the Earth’s velocity relative to the Dark Matter halo on the central date of the observation period [10].

velocity and/or in large recoil angles would be strongly suppressed.

Meanwhile, the angular recoil-direction/energy distributions of several target nuclei in the laboratory coordinate system were also presented in this paper, since this 3-D information, combined with the recoil spectrum, could practically be measured in directional direct DM detection experiments. Our simulations showed that, on one hand, for one given target nucleus, the heavier its mass, the more obvious the (qualitative) differences between the angular distribution patterns simulated with different WIMP masses; on the other hand, the larger the mass difference between two target nuclei (and the larger the WIMP mass), the larger the pattern differences between their angular distributions. This indicates that, by comparing and/or combining the (quantitative) nuclear recoil flux and energy or even only their (qualitative) distribution patterns with the same/different target nuclei (provided from different underground laboratories), one could constrain/identify the mass (range) of halo WIMPs.

Furthermore, since, considering the very low theoretically estimated event rate, combining and analyzing WIMP scattering events provided with the same target nucleus from different underground laboratories in a laboratory/location-independent coordinate system would be practically a very useful strategy, we also demonstrated the angular distributions of the recoil direction/energy in the Equatorial coordinate system. While the anisotropies of the distribution patterns of the recoil direction/energy could be observed clearly, neither the centers of the most

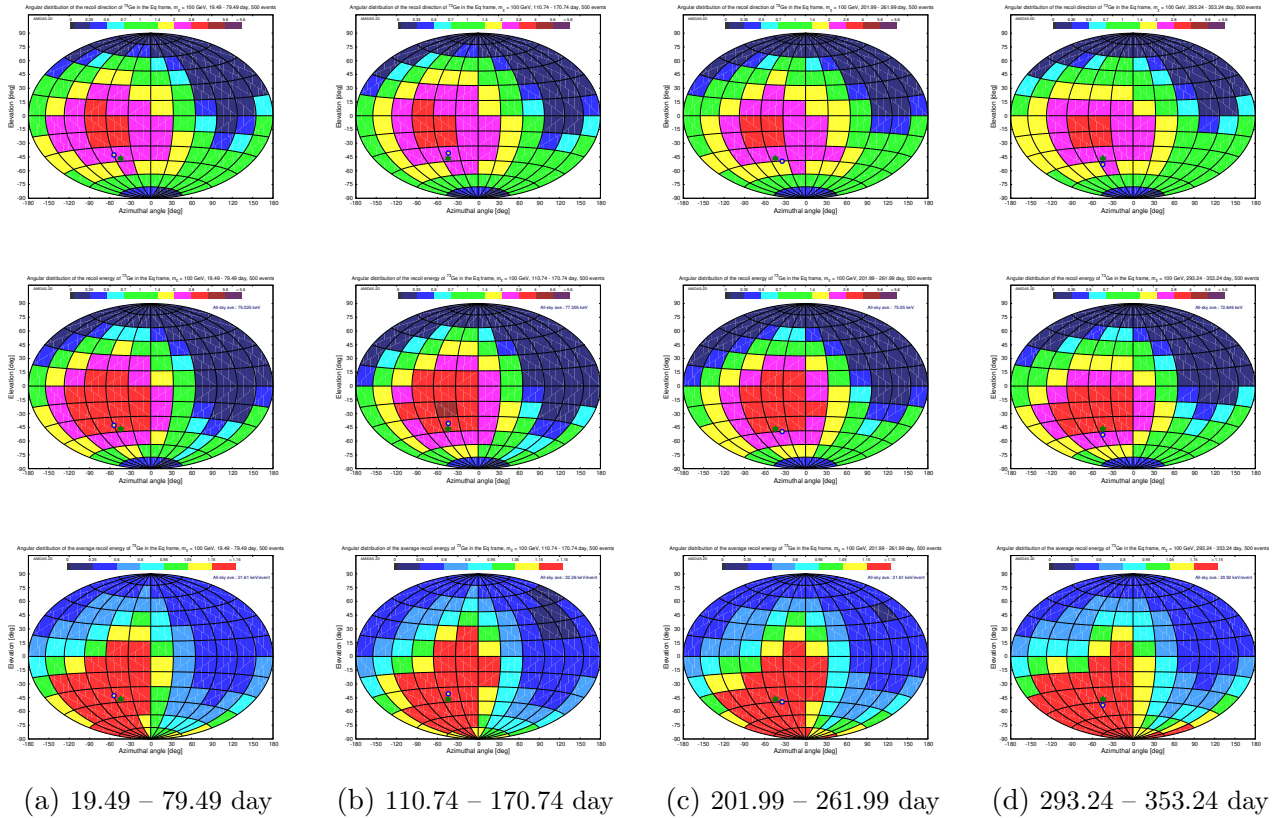


Figure 25: As in Figs. 24, except that a middle-mass nucleus ^{73}Ge has been considered as our target.

frequent recoil directions nor those of the most energetic ones of all simulated target nucleus–WIMP mass combinations could match the theoretical main direction of the WIMP wind, but have clearly northerly shifts, which increase with the increased mass of the target nucleus and/or incident WIMPs. Interestingly, the hot-points of the angular distributions of the average recoil energy seem to be approximately centered around the theoretical main direction of incident WIMPs, with nevertheless some small (but observable) target/WIMP-mass dependent pattern differences.

Since the original purpose of directional direct Dark Matter detection experiments is to observe the directionality (the diurnal modulated anisotropy) of the recoil direction of WIMP–nucleus scattering events, we demonstrated equivalently the annual modulated anisotropies of the distribution patterns of the recoil direction (flux)/energy of the scattered target nuclei in the incoming–WIMP and the Equatorial coordinate systems. Our simulations showed that, firstly, more scattered target nuclei would go to smaller (larger) recoil angles with larger (smaller) recoil energies in the advanced summer (winter). Secondly, while the angular distribution patterns of the average recoil energy show indeed approximately circular clockwise rotations following the instantaneous theoretical main direction of the incident halo WIMPs, the approximate rotation centers of the distribution patterns of the recoil direction and the accumulated recoil energy would clearly shift northwesterly. Moreover, the annual variations of the angular recoil–direction distributions of middle-mass and heavy target nuclei seem not to be circular, but oscillated somehow latitudinally. And the shapes of the most frequent recoil directions seem also to be somehow longitudinally squeezed; the heavier the nuclear (and/or the WIMP) mass, the stronger the pattern distortion would be. So far we have no reasonable explanation(s) for this

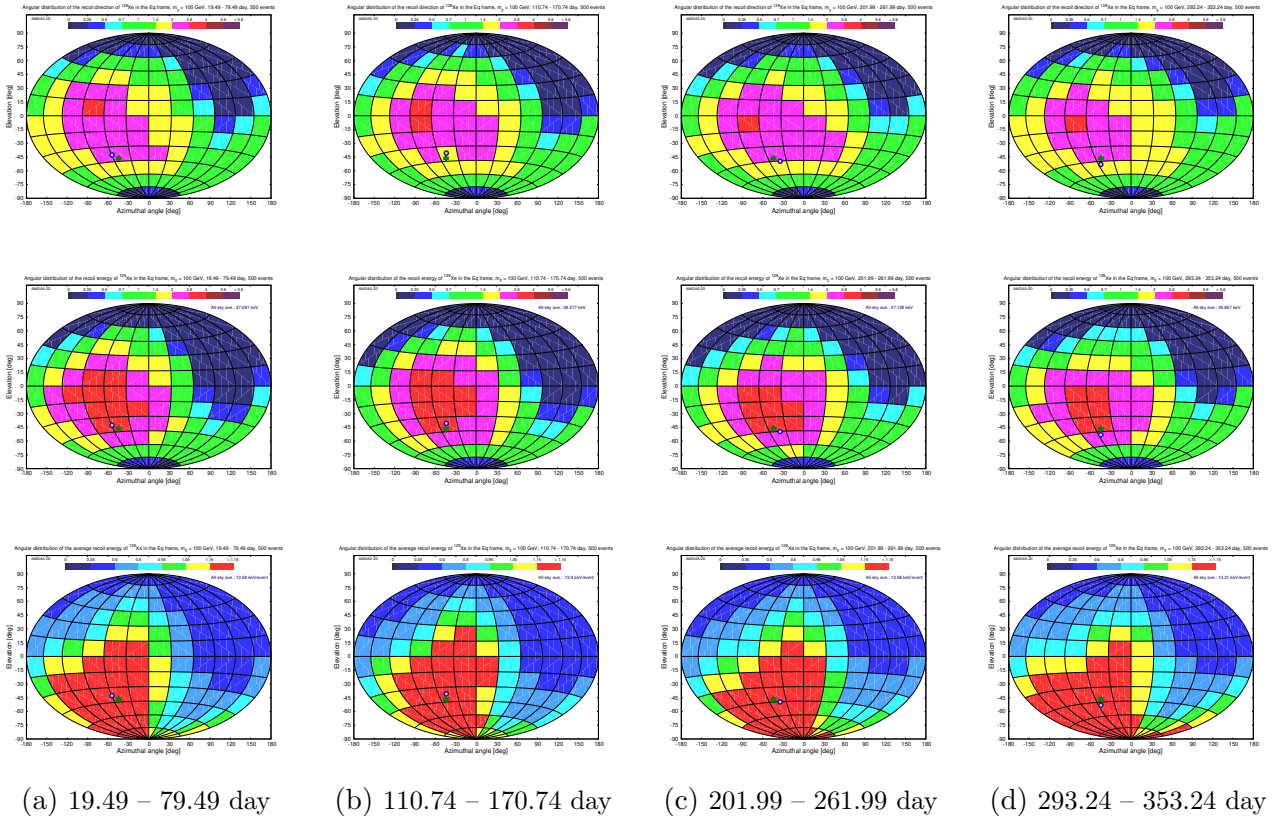


Figure 26: As in Figs. 24 and 25, except that a heavy nucleus ^{129}Xe has been considered as our target.

(unexpected) observations.

In our simulations presented in this paper, 500 accepted WIMP–scattering events on average in one observation period (365 days/year or 60 days/season) in one experiment for one laboratory/target nucleus have been simulated. Regarding the observation periods considered in our simulations presented in this paper, we used several approximations about the Earth’s orbital motion in the Solar system. First, the Earth’s orbit around the Sun is perfectly circular on the Ecliptic plane and the orbital speed is thus a constant. Second, the date of the vernal equinox is exactly fixed at the end of the May 20th (the 79th day) of a 365-day year and the few extra hours in an actual Solar year have been neglected. Nevertheless, considering the very low WIMP scattering event rate and thus maximal a few (tens) of total (combined) WIMP events observed in at least a few tens (or even hundreds) of days (an optimistic overall event rate of $\lesssim \mathcal{O}(1)$ event/day) for the first–phase analyses, these approximations should be acceptable.

In summary, we finally achieved the full Monte Carlo scattering–by–scattering simulation of the 3-dimensional elastic WIMP–nucleus scattering process and can provide experimentally measurable (pseudo)data: the 3-dimensional recoil direction and the recoil energy of the WIMP–scattered target nuclei. Several important (but unexpected) characteristics have been observed. Hopefully, this (and more works fulfilled in the future) could help our colleagues to develop analysis methods for understanding the astrophysical and particle properties of Galactic WIMPs as well as the structure of Dark Matter halo by using directional direct detection data.

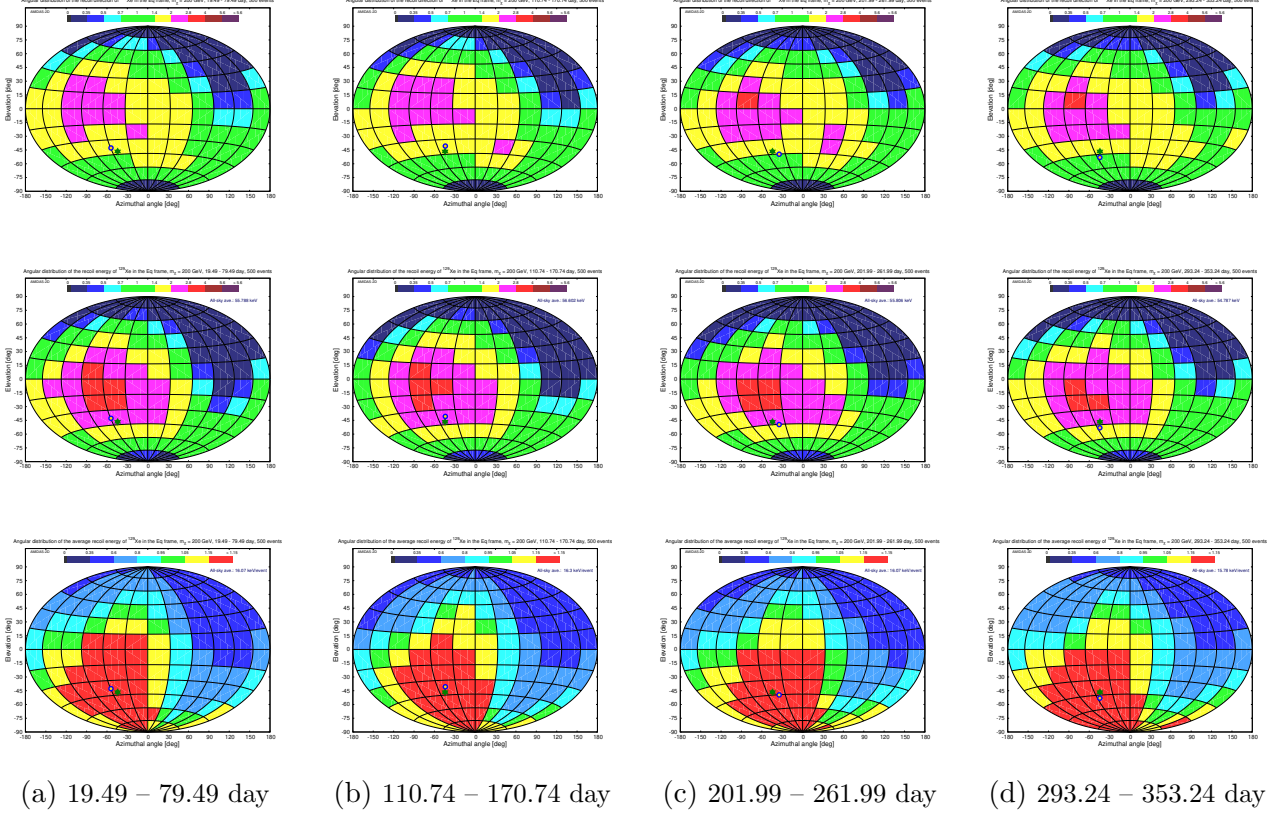


Figure 27: As in Figs. 26: ^{129}Xe has been considered as the target nucleus, except that the mass of incident WIMPs has been considered as heavy as $m_\chi = 200$ GeV.

Acknowledgments

The author would like to thank the pleasant atmosphere of the W101 Ward and the Cancer Center of the Kaohsiung Veterans General Hospital, where part of this work was completed. This work was strongly encouraged by the “*Researchers working on e.g. exploring the Universe or landing on the Moon should not stay here but go abroad.*” speech.

References

- [1] G. Jungman, M. Kamionkowski and K. Griest, “*Supersymmetric Dark Matter*”, *Phys. Rep.* **267**, 195–373 (1996), [arXiv:hep-ph/9506380](#).
- [2] R. J. Gaitskell, “*Direct Detection of Dark Matter*”, *Ann. Rev. Nucl. Part. Sci.* **54**, 315–359 (2004).
- [3] L. Baudis, “*Direct Dark Matter Detection: the Next Decade*”, Issue on “*The Next Decade in Dark Matter and Dark Energy*”, *Phys. Dark Univ.* **1**, 94–108 (2012), [arXiv:1211.7222](#) [astro-ph.IM].
- [4] L. Baudis and S. Profumo, contribution to “*The Review of Particle Physics 2020*”, *Prog. Theor. Exp. Phys.* **2020**, 083C01 (2020), *27. Dark Matter*.

- [5] S. Ahlen *et al.*, “*The Case for a Directional Dark Matter Detector and the Status of Current Experimental Efforts*”, *Int. J. Mod. Phys. A* **25**, 1–51 (2010), [arXiv:0911.0323 \[astro-ph.CO\]](#).
- [6] F. Mayet *et al.*, “*A Review of the Discovery Reach of Directional Dark Matter Detection*”, *Phys. Rept.* **627**, 1–49 (2016), [arXiv:1602.03781 \[astro-ph.CO\]](#).
- [7] J. B. R. Battat *et al.*, “*Readout Technologies for Directional WIMP Dark Matter Detection*”, *Phys. Rept.* **662**, 1–46 (2016), [arXiv:1610.02396 \[physics.ins-det\]](#).
- [8] CYGNUS Collab., S. E. Vahsen *et al.*, “*CYGNUS: Feasibility of a Nuclear Recoil Observatory with Directional Sensitivity to Dark Matter and Neutrinos*”, [arXiv:2008.12587 \[physics.ins-det\]](#) (2020).
- [9] S. E. Vahsen, C. A. J. O’Hare and D. Loomba, “*Directional Recoil Detection*”, *Ann. Rev. Nucl. Part. Sci.* **xx**, 1–45 (2021), [arXiv:2102.04596 \[physics.ins-det\]](#).
- [10] C.-L. Shan, “*Simulations of the 3-Dimensional Velocity Distribution of Halo Weakly Interacting Massive Particles for Directional Dark Matter Detection Experiments*”, [arXiv:1905.11279 \[astro-ph.HE\]](#) (2019), in publication.
- [11] C.-L. Shan, “*Simulations of the Angular Kinetic–Energy Distribution of Halo Weakly Interacting Massive Particles for Directional Dark Matter Detection Experiments*”, in publication.
- [12] C.-L. Shan, “*Monte Carlo Scattering–by–Scattering Simulation of 3-Dimensional Elastic WIMP–Nucleus Scattering Events*”, [arXiv:2103.xxxxx \[hep-ph\]](#) (2021).
- [13] C.-L. Shan, “*3-Dimensional Effective Velocity Distribution of Halo Weakly Interacting Massive Particles Scattering off Nuclei in Direct Dark Matter Detectors*”, [arXiv:2103.xxxxx \[astro-ph.HE\]](#) (2021).
- [14] C.-L. Shan, online interactive demonstrations of 3-dimensional WIMP–nucleus elastic scattering for (directional) direct Dark Matter detection experiments and phenomenology, <http://www.tir.tw/phys/hep/dm/amidas-2d/> (2021).
- [15] Agua Negra Deep Experiment Site (ANDES), see <http://andeslab.org/>.
- [16] A. Bandyopadhyay and D. Majumdar, “*On Diurnal and Annual Variations of Directional Detection Rates of Dark Matter*”, *Astrophys. J.* **746**, 107 (2012), [arXiv:1006.3231 \[hep-ph\]](#).